

COMPARISON OF NOTCH DEPTH FOR CONSTRAINED LEAST MEAN SQUARES
AND DOMINANT MODE REJECTION BEAMFORMERS

by

Mani Shanker Krishna Bojja

A Thesis

Submitted to the

Graduate Faculty

of

George Mason University

In Partial fulfillment of

The Requirements for the Degree

of

Master of Science

Electrical Engineering

Committee:

_____ Dr. Kathleen E. Wage, Thesis Director

_____ Dr. Jill K. Nelson, Committee Member

_____ Dr. Janos Gertler, Committee Member

_____ Dr. Monson Hayes, Chairman, Department
of Electrical and Computer Engineering

_____ Dr. Kenneth S. Ball, Dean for
Volgenau School of Engineering

Date: _____ Spring Semester 2015
George Mason University
Fairfax, VA

Comparison of Notch Depth for Constrained Least Mean Squares and Dominant Mode
Rejection Beamformers

A thesis submitted in partial fulfillment of the requirements for the degree of
Master of Science at George Mason University

By

Mani Shanker Krishna Bojja
Bachelor of Science
K.S.Raju Institute of Technology and Sciences, 2011

Director: Dr. Kathleen E. Wage, Associate Professor
Department of Electrical and Computer Engineering

Spring Semester 2015
George Mason University
Fairfax, VA

Copyright © 2015 by Mani Shanker Krishna Bojja
All Rights Reserved

Dedication

I dedicate this thesis to my dear and loving parents Veeresh and Sunitha, respected Professor Kathleen E Wage and reliable friends Mehdi Farrokhrooz, Le Thuykhanh. Thanks dad for teaching me principles like desire to achieve, setting your own limits and working hard while being punctual. Thanks mom for teaching me to be persistent and disciplined at my work. Thank you Professor Kathleen E Wage for teaching me not only the subject knowledge, but also teaching me intangible things such as thinking of a solution oriented way, learning from my mistakes and counseling me on all sectors of life in each and every meet. Last but not the least, I would like to thank my colleagues, Mehdi and Le, for helping me all through the process and teaching me. I am very blessed to have such an amazing people teaching me through long. Thank you.

Table of Contents

	Page
List of Tables	v
List of Figures	vi
Abstract	ix
1 Introduction	1
2 Background	3
2.1 Terminology and structure of beamformer	3
2.2 Steepest Descent	7
2.3 Frost LMS Algorithm	8
2.4 DMR algorithm	12
3 Empirical Study of the Single Interferer Case	15
3.1 Simulation Parameters	15
3.2 Analysis of Steepest Descent Beamformer	17
3.3 Analysis of Frost LMS Beamformer	18
3.3.1 ND performance of Frost LMS beamformer	18
3.3.2 White Noise Gain for Frost LMS beamformer	25
3.4 Analysis of N-LMS beamformer	31
3.5 Comparison of LMS and DMR beamformers	38
3.6 Summary	45
4 Empirical Study of a Multi Interferer Case	46
4.1 Multiple Interferers Simulation Environment	46
4.2 Results of N-LMS beamformer	46
4.3 Comparison of N-LMS and ER-DMR beamformers	51
4.3.1 Comparison based on Notch Depth	51
4.3.2 Comparison based on White Noise Gain	51
4.4 Computational Complexity of N-LMS and ER-DMR	53
4.5 Summary	55
5 Conclusion	56
Bibliography	58

List of Tables

Table		Page
4.1	Comparison of FLOPS count between N-LMS AND ER-DMR	53
4.2	Theoretical Calculation of Multiplication factor for NLMS and ER-DMR . .	55
4.3	Execution time comparison of NLMS and ER-DMR	55

List of Figures

Figure	Page
2.1 Diagram of the basic beamformer. The input signal data is collected from the N sensors and is passed through a filter with weights stored in \mathbf{w}	4
2.2 Comparison of the beampatterns for the conventional and MVDR beamformers	6
3.1 ND vs. snapshots for SD algorithm. Each curve uses different μ values. All the curves are considered with 40 dB INR at the input	17
3.2 ND vs. snapshots for Frost LMS algorithm. Different curves represent different INR levels namely 40 dB, 20 dB, 0 dB. All the curves are considered with a constant mu value of 0.000001	18
3.3 ND vs. snapshots for Frost LMS algorithm for a standard case with three different INR levels namely 0 dB, 20 dB and 40 dB. A one degree less than the maximum possible step size is used as μ for simulation purposes.	20
3.4 ND vs. snapshots for Frost LMS algorithm. Different curves represent different mu values used. All the curves are assume a 40 dB INR interferer . .	21
3.5 SSND vs. μ comparison between Frost LMS and MVDR algorithms.	23
3.6 SSND vs μ comparison between 40 dB, 37 dB and 20 dB INRs.	24
3.7 SSND vs μ comparison between 20 dB and 10 dB INRs.	25
3.8 SSND vs μ comparison between 10 dB and 2 dB INRs.	26
3.9 Curve fitting of SSND vs. μ with ND values obtained by using different INRs at the input. A least squares fit method is used to fit the curve.	27
3.10 Comparison of WNG of CBF, MVDR, SD and Frost LMS (with three different μ 's namely 0.01, 0.001 and 0.0001) for a 0 dB INR	28
3.11 Comparison of WNG of CBF, MVDR, SD and Frost LMS (with three different μ 's namely 0.0001, 0.00001 and 0.000001) for a 20 dB INR	29
3.12 Comparison of WNG of CBF, MVDR, SD and Frost LMS (with three different μ 's namely 0.000001, 0.0000001 and 0.00000001) for a 40 dB INR	30
3.13 Comparison of ND of CBF and Frost LMS (with μ of 0.01) for 0 dB INR . .	31

3.14	ND vs. snapshots for a N- LMS algorithm, with a variable μ , for different INRs namely 40 dB, 20 dB, 0 dB. Here the values of $\kappa = 1$ and $\varsigma = 1$. . .	33
3.15	Comparing the mean and variance of SSND of Frost LMS and N-LMS at 10000th.	34
3.16	ND vs. snapshots for a N-LMS algorithm, with a variable μ , only with 40 dB INR as input to the beamformer. Here the three curves represent three different κ values namely 1,0.1,0.01	35
3.17	Comparison of ND vs snapshots of Frost LMS ($\mu = 5.0e-07$) and N-LMS ($\kappa = 0.05$) with 40 dB INR at the input	37
3.18	ND vs. snapshots comparison of FR-DMR and ER-DMR. The input to the beamformer is a -10 dB interferer and white noise.	39
3.19	ND vs. snapshots comparison of FR-DMR and ER- DMR. The input to the beamformer is a 40 dB interferer and white noise.	40
3.20	ND vs. snapshots comparison of N-LMS (variable μ) and ER-DMR (with rank estimation). The input to the beamformer is a 40 dB interferer. The N-LMS is considered with three different κ values namely 1, 0.1, 0.01	41
3.21	WNG comparison of N-LMS and ER-DMR for the standard single interferer case with 40 dB INR as input.	43
3.22	WNG comparison of N-LMS for the standard single interferer case with three INRs 0 dB, 20 dB and 40 dB. κ and sigma values are 1 and 1 respectively. .	44
4.1	CBF beampattern with direction of arrival of different interferers. Four interferers arriving from direction corresponding to the u values of 0.06, 0.1, 0.14 and 0.18	47
4.2	ND vs. snapshots performance comparison for robust LMS for the case of single and multiple interferers. Three different configurations of multiple interferers are used with four different INR power levels. All the interferers are incident from four consecutive peak side lobes of the CBF.	48
4.3	ND vs. snapshots performance comparison for ER-DMR for the case of single and multiple interferers. Three different configurations of multiple interferers are used with four different INR power levels All the interferers are incident from four consecutive peak side lobes of the CBF.	49

4.4	ND vs. snapshots performance comparison of ER-DMR and N-LMS for the case of multiple interferers. Four different INR power levels at four consecutive peak side lobes of the CBF. 40 dB, 20 dB, 30 dB and 0 dB INR's are used in the first comparison. 40 dB, 40 dB, 40 dB and 40 dB INRs are used in the second comparison.	52
4.5	WNG vs. snapshots, cost comparison of ER-DMR and N-LMS for the case of multiple interferers. Four different INR power levels at four consecutive peak side lobes of the CBF.	54

Abstract

COMPARISON OF NOTCH DEPTH FOR CONSTRAINED LEAST MEAN SQUARES AND DOMINANT MODE REJECTION BEAMFORMERS

Mani Shanker Krishna Bojja, M.S.

George Mason University, 2015

Thesis Director: Dr. Kathleen E. Wage

Detection of low power signals in the presence of high power interferers is a common problem in spatial signal processing. Notch depth (ND) is defined as the response of the beamformer in the interferer direction when the beamformer is steered towards a specified look direction. This thesis analyzes the ND of the constrained Least Mean Squares algorithm proposed by Frost [1]. Several variants of the LMS algorithm are considered, and the algorithm is analyzed for the case of single and multiple interferers. The thesis compares the ND of the LMS beamformer to the ND of the Dominant Mode Rejection beamformer proposed by Abraham and Owsley [2]. The performance comparison indicates that DMR attains a deeper notch faster than LMS. The white noise gain of the two beamformers is approximately the same. Analysis of the computational complexity of the LMS and DMR algorithms indicates that DMR requires on the order of N times more floating point operations than LMS, where N is the size of the receiving array. Thus, DMR is a better choice for applications requiring fast convergence as long as the processor can handle the increased computational load.

Chapter 1: Introduction

In sonar array processing the need to detect low power signals in the presence of high power noise is a persistent problem. Initial development was made to understand and solve this problem by using optimum Minimum Variance Distortionless (MVDR) beamformer [3], which assumes known signal characteristics and is the most basic adaptive beamformer. Later the study was extended developing other adaptive algorithms in detecting such low power signals with changing power characteristics. One such algorithms have already been analyzed in the simple case of single interferer and noise, namely the Dominant Mode Rejection (DMR) [4] algorithm. This thesis is focused on understanding the performance of Frost Least Mean Squares (LMS) [1] algorithm by presenting numerical results based on the characteristic called Notch Depth (ND).

ND is a measure of how well a beamformer can eliminate an interferer. A deeper notch implies that the beamformer filters out more of the interference, thus improving its output signal-to-interference-plus-noise (SINR) ratio. The beamformer which achieves optimum ND is the MVDR beamformer implemented using the ensemble covariance matrix (ECM). The MVDR beamformer minimizes the total variance of the output of the beamformer while maintaining a distortionless constraint in the desired direction. The Frost LMS and Dominant Mode Rejection algorithm (DMR) are adaptive beamformers which use the Sample Covariance Matrix (SCM), an estimate of the ECM, to do the beamforming. Essentially, the goal of adaptive beamformers is to approximate the performance of the optimum beamformer.

The DMR Adaptive Beamformer (ABF) is a reduced rank subspace algorithm, which constructs its weight vector using a structured covariance estimate, obtained from an eigen-decomposition of the SCM. The rank here refers to the number planewave interferers approaching the array. Wage and Buck [5] present comprehensive results on the behavior of ND for the DMR algorithm. Firstly, empirical data demonstrates that the DMR continues to place a deeper notch for increased number of snapshots, where snapshots is defined as the independent samples obtained at the input, until it reaches a threshold and then levels out. In addition, Wage and Buck [6] derived a theoretical equation of the SINR loss for the DMR ABF using the Random Matrix Theory (RMT). SINR loss governs the rate of convergence of DMR to the optimal MVDR beamformer. Secondly, a theoretical equation is derived depicting the dependence of White Noise Gain (WNG) on the interferer location, with respect to look direction.

The goal of this thesis is to characterize the notch depth of the Frost LMS beamformer and to analyze the conditions under which it attains the optimal notch depth of MVDR beamformer. Frost LMS algorithm is a gradient based algorithm that forms its weight vector by imposing a unity gain constraint in the look direction. Primarily, the idea is to compare the results in the DMR paper [4] to the Frost LMS [1] algorithm by performing a similar analysis for a standard single interferer standard case. Secondly, the focus is to expand this study to more complex cases like the presence of multiple interferers at the input.

This thesis is organized as follows. Chapter 2 reviews background material and defines the Steepest Descent (SD), Frost LMS, and DMR beamformers. Chapters 3 and 4 compare the performance of the Frost LMS and DMR beamformers for single and multiple interferer cases, respectively. Finally, Chapter 5 summarizes the results and indicates directions for further research.

Chapter 2: Background

2.1 Terminology and structure of beamformer

Fig. 2.1 shows the array configuration used throughout the thesis. The array has N sensors with an equal spacing of $\lambda/2$, where λ is the wavelength of the input narrowband signal. The sensors are oriented along the z axis. The input is the sum of a planewave interferers and independent spatially white sensor noise. The interferer arrives at an angle θ_i , defined as the angle measured with respect to the positive z axis. The signal $\mathbf{p}(l)$ represents the resulting narrowband signal recorded at the sensors at the l^{th} snapshot. A planewave signal coming from a particular direction is represented by a replica vector \mathbf{v} that depends on the angle of arrival as follows:

$$\mathbf{v}_i = \mathbf{v}(\theta_i) = \begin{bmatrix} e^{j\frac{2\pi}{\lambda} \cos(\theta_i)z_1} \\ \vdots \\ e^{j\frac{2\pi}{\lambda} \cos(\theta_i)z_N} \end{bmatrix} \quad (2.1)$$

. The signal $\mathbf{p}(l)$ is represented as follows:

$$\mathbf{p}(l) = \sum_{i=1}^D b_i(l)\mathbf{v}_i + \mathbf{n}, \quad (2.2)$$

where $b_i(l)$ is complex circular random variable at l^{th} snapshot. A complex circular random variable has mean zero and variance equal to the sum of the variances of the real and imaginary section of a complex random variable, where the real and imaginary parts are uncorrelated. \mathbf{n} is the noise at the input and \mathbf{v}_i represents the plane wave replica vector.

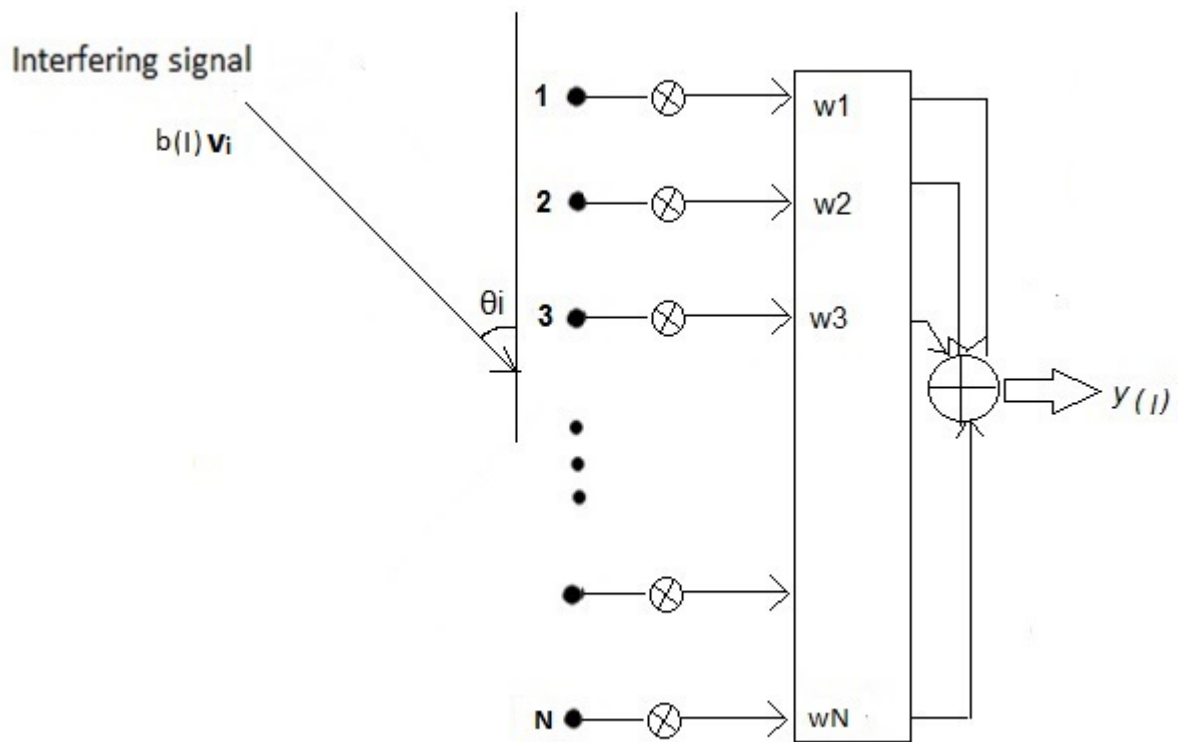


Figure 2.1: Diagram of the basic beamformer. The input signal data is collected from the N sensors and is passed through a filter with weights stored in \mathbf{w} .

The beamformer described above is a spatial filter, which processes the signal $\mathbf{p}(l)$ obtained from a set of sensors through the weights $\mathbf{w}(l)$ to obtain a desired output $y(l)$:

$$y(l) = \mathbf{w}(l)^H \mathbf{p}(l). \quad (2.3)$$

From Eq. 2.3 it is clear that the structure of the weights $\mathbf{w}(l)$ governs the output of the beamformer at each l^{th} snapshot. In order to understand the effect of the structure of \mathbf{w} on the output, consider two different weight vectors namely, the weight vectors of the Conventional Beamformer (CBF) in Eq. 2.4 and the MVDR [3] beamformer Eq. 2.8. The weight vector of the conventional beamformer is a scaled version of the replica vector of the steering direction \mathbf{v}_m :

$$\mathbf{w}_{conv} = (\mathbf{v}_m^H \mathbf{v}_m)^{-1} \mathbf{v}_m. \quad (2.4)$$

The CBF is guaranteed to have unity gain in the steering direction. The MVDR weight vector is obtained by minimizing the power at the output of the beamformer while maintaining a unity gain constraint in the steering direction in the direction, defined by \mathbf{v}_m . Here the power is defined as the expected absolute value squared of the beamformer output, i.e.,

$$OutputPower = E(|y(l)|^2) = E(\mathbf{w}(l)^H \mathbf{p} \mathbf{p}^H \mathbf{w}(l)). \quad (2.5)$$

The optimization problem is as follows:

$$minimize \quad (\mathbf{w}(l)^H \mathbf{\Sigma} \mathbf{w}(l)) \quad (2.6)$$

$$subject \ to \quad \mathbf{w}(l)^H \mathbf{v}_m = 1. \quad (2.7)$$

Solving the above equations for \mathbf{w}_{mvdr} by the method Lagrange multipliers leads to the following solution:

$$\mathbf{w}_{mvdr} = (\mathbf{v}_m \mathbf{\Sigma}^{-1} \mathbf{v}_m)^{-1} \mathbf{\Sigma}^{-1} \mathbf{v}_m. \quad (2.8)$$

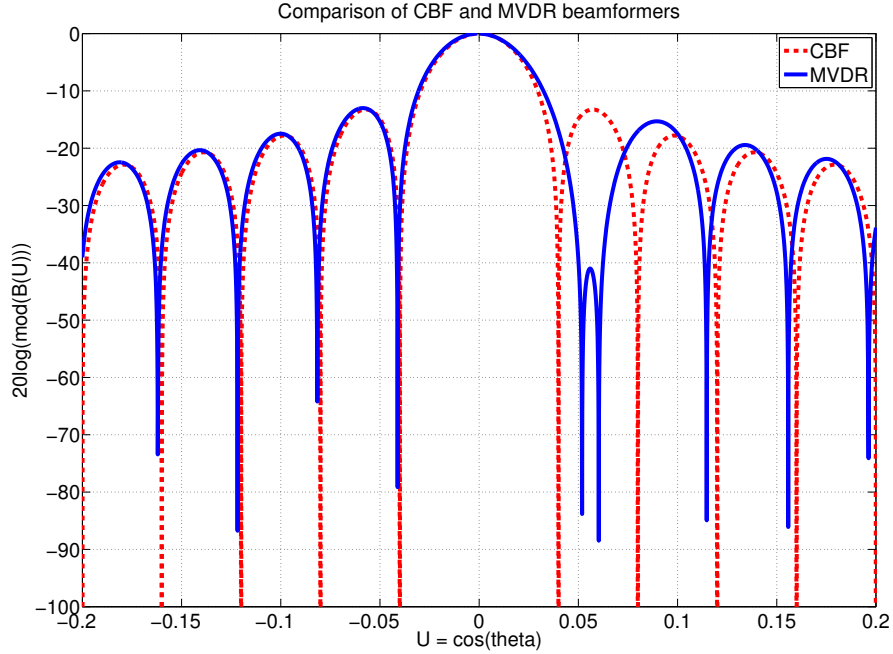


Figure 2.2: Comparison of the beampatterns for the conventional and MVDR beamformers

In order to better understand the behavior of the conventional and MVDR weight vector, consider their beampatterns. The beampattern is defined as the absolute value squared at the output of the beamformer:

$$ND = B(\theta_i) = |\mathbf{w}^H \mathbf{v}_i|^2, \quad (2.9)$$

where $B(\theta_i)$ is the value of the beampattern evaluated in θ_i in direction. The beampattern Eq. 2.9 quantifies the response of the beamformer to a planewave, arriving at the array of sensors at a particular angle.

Consider a simulation to illustrate the difference in the CBF and MVDR beamformers. The number of sensors in the simulation is $N = 50$ and the array has half-wavelength spacing. There is a single interferer with interference to noise ratio (INR) equal to 40 dB. The interferer is located at the peak sidelobe of the conventional beamformer, i.e.,

at $u = \cos(\theta_i) = 0.06$. Fig. 2.2 compares the beampatterns of the CBF and MVDR beamformers. The plot shows that the MVDR weight vector successfully places a notch of $ND = -127$ dB in the direction of the interferer, while the conventional weight vector does not place a notch in the direction of the interferer. However, both beamformers preserve the unity gain constraint in the steering direction ($u = \cos(90) = 0$). The MVDR beamformer implemented for Fig. 2.2 assumes that the ECM is available to compute the weights. In practice, this is not true and the weight vector must be designed using sample statistics. The Frost LMS and DMR algorithms considered in this thesis both use sample statistics.

White Noise Gain (WNG) is another important characteristic used to measure the performance of the algorithm. WNG in Eq. 2.10 is the gain in signal power, measured in Signal to Noise Ratio (SNR), provided by the beamformer with white noise at the beamformer input:

$$\text{WNG} = 1/\mathbf{w}^H \mathbf{w}. \quad (2.10)$$

The WNG for CBF is $10\log_{10}(N)$ which is approximately 17dB for the CBF for the $N=50$ example. The MVDR beamformer shows a slight loss in WNG, down to 16.8 dB. This is the price paid to steer a deep notch in the interferer direction.

The following sections reviews the theoretical formulation of Frost LMS and DMR weight vectors. Moving forward empirical results are presented in the next two chapters.

2.2 Steepest Descent

The Frost LMS algorithm is a gradient based algorithm that uses input samples to compute the weight vector. The gradient descent algorithm that assumes known signal and noise characteristics is the Steepest Descent (SD) algorithm [7]. SD helps in formulating the

Frost LMS algorithm. The weight vector of the SD algorithm is defined as:

$$\mathbf{w}(l+1) = \mathbf{P}_\perp[\mathbf{w}(l) - \mu \boldsymbol{\Sigma} \mathbf{w}(l)] + \mathbf{w}_q, \quad (2.11)$$

where the weight vector of the conventional beamformer is

$$\mathbf{w}_q = \mathbf{w}(0) = \mathbf{v}_m (\mathbf{v}_m^H \mathbf{v}_m)^{-1} \quad (2.12)$$

and the projection matrix orthogonal to the look direction replica vector is \mathbf{P}_\perp

$$\mathbf{P}_\perp = \mathbf{I} - \mathbf{v}_m (\mathbf{v}_m^H \mathbf{v}_m)^{-1} \mathbf{v}_m^H. \quad (2.13)$$

$\boldsymbol{\Sigma}$ is the ensemble covariance matrix. The SD algorithm is an optimum minimum mean squared error estimate of the weight vector \mathbf{w} and assumes that the statistics of the input are known a priori, which is certainly not true in practical situations. Moreover, if the statistics were known there wouldn't be any need for an adaptive technique to find the optimum weight vector \mathbf{w} .

2.3 Frost LMS Algorithm

The Frost LMS algorithm is a stochastic gradient version of the SD algorithm as defined in Eq. 2.11. The Frost LMS [1] algorithm calculates the instantaneous weights adaptively, such that it minimizes the total power at the output while maintaining a unity gain constraint in the look direction. Unlike the SD beamformer, the Frost algorithm does not assume that the ensemble statistics are available.

Frost has formulated the equation for LMS in [1] by minimizing the total variance at the output of the beamformer, i.e.,

$$\text{minimize } (\mathbf{w}^H \mathbf{p}(l) \mathbf{p}(l)^H \mathbf{w}) \quad (2.14)$$

while maintaining a unity gain constraint the steering direction,

$$\mathbf{w}^H \mathbf{v}_m = 1. \quad (2.15)$$

Using the above conditions and forming the Lagrangian equation leads to:

$$J = \mathbf{w}^H \mathbf{p}(l) \mathbf{p}(l)^H \mathbf{w} + \lambda (\mathbf{w}^H \mathbf{v}_m - 1) + \lambda^* (\mathbf{w} \mathbf{v}_m^H - 1) \quad (2.16)$$

where \mathbf{v}_m is the replica vector associated with the angle of arrival of the source signal. Initializing the weight vector with the weights of a conventional beamformer, an adaptive iteration is performed in finding the next weight vector by moving in the direction of negative gradient of J in the order to reach the optimum. Solving for the weight vector leads to

$$\mathbf{w}(l+1) = \mathbf{P}_\perp [\mathbf{w}(l) - \mu \mathbf{p}(l) \mathbf{p}(l)^H \mathbf{w}(l)] + \mathbf{w}_q, \quad (2.17)$$

where $\mathbf{w}(l)$ is the weight vector at l^{th} time instant, \mathbf{w}_q is the conventional weight vector and \mathbf{P}_\perp is the orthogonal projection matrix. It can be observed from the Eq 2.17 that in the Frost LMS algorithm, the instantaneous covariance matrix $\mathbf{p}(l) \mathbf{p}(l)^H$ replaces the Ensemble Σ in SD.

The step size parameter μ controls the rate of convergence of the Frost LMS algorithm. In order to understand the behavior of weight vector of Frost LMS effectively, a constant μ value is assumed such that stability is maintained in the LMS algorithm. Monzingo [8] has derived the stable range of step size μ . Monzingo [8] derived this range by minimizing the variation of weight vector $\mathbf{w}(t)$ of SD from the optimum weight vector \mathbf{w}_{mvdrr} by using error vector $\boldsymbol{\varepsilon}(t)$ [9]:

$$\boldsymbol{\varepsilon}(t+1) = \mathbf{w}(t+1) - \mathbf{w}_{mvdrr}. \quad (2.18)$$

As time t increases the goal is to minimize this error such that the performance of SD achieves that of the MVDR. This minimization of $\boldsymbol{\varepsilon}(t)$ leads to the derivation of the range of μ as discussed in [8]. Substituting SD weight vector Eq. 2.11 in Eq. 2.18 and simplifying it, results in:

$$\boldsymbol{\varepsilon}(t+1) = \mathbf{P}_\perp \boldsymbol{\varepsilon}(t) - \mu \mathbf{P}_\perp \boldsymbol{\Sigma} \boldsymbol{\varepsilon}(t). \quad (2.19)$$

Multiplying the expression in 2.19 by projection matrix, \mathbf{P}_\perp , and expressing in terms of initial error vector $\boldsymbol{\varepsilon}(0)$ leads to:

$$\boldsymbol{\varepsilon}(t+1) = [\mathbf{I} - \mathbf{P}_\perp \boldsymbol{\Sigma} \mathbf{P}_\perp]^{t+1} \boldsymbol{\varepsilon}(0). \quad (2.20)$$

The term in the braces of Eq. 2.20 determines the convergence of the error vector to zero. Let the projection of eigenvectors of ECM be represented by the new eigenvector matrix:

$$\mathbf{U} = \mathbf{P}_\perp \boldsymbol{\Xi}. \quad (2.21)$$

Using this fact in Eq. 2.21 to express initial error vector $\boldsymbol{\varepsilon}(0)$ in terms of the new eigenvector matrix \mathbf{U} leads to:

$$\boldsymbol{\varepsilon}(0) = \sum_{i=1}^N c_i \mathbf{u}_i \quad (2.22)$$

$$\boldsymbol{\varepsilon}(t+1) = \mathbf{U}(\mathbf{I} - \mu \boldsymbol{\Gamma})^{t+1} \mathbf{c}. \quad (2.23)$$

Substituting initial error vector $\boldsymbol{\varepsilon}(0)$ in Eq. 2.20 gives rise to Eq. 2.24:

$$\boldsymbol{\varepsilon}(t+1) = \sum_{i=1}^N (1 - \mu \gamma_i)^{t+1} c_i \mathbf{u}_i. \quad (2.24)$$

Finally, the error vector from Eq. 2.24 converges to zero, only when $|1 - \mu\gamma_i|$ is less than 1:

$$|1 - \mu\gamma_i| < 1 \implies -1 < 1 - \mu\gamma_i < 1, \quad (2.25)$$

$$\implies \mu < 2/(\gamma_i)_{max}. \quad (2.26)$$

The above condition constraints μ to be less than $2/(\gamma_i)_{max}$. If the μ is larger than $2/(\gamma_i)_{max}$ then the error vector in Eq. 2.24 approaches infinity and making the algorithm go unstable. Thus, the maximum step size, $2/(\gamma_i)_{max}$ acts as a boundary in order for the algorithm to be stable.

As mentioned in [3], LMS algorithm can be made adaptive by making the μ dependent on the instantaneous input to the sensor array. N-LMS algorithm computes the weight vector using a variable $\mu(l)$ as presented:

$$\mu(l) = \frac{\kappa}{\varsigma + \mathbf{p}(l)^H \mathbf{p}(l)}. \quad (2.27)$$

In addition to the input power $\mathbf{p}(l)^H \mathbf{p}(l)$, which makes the system adaptive, two constants namely κ and ς in the numerator and denominator respectively are introduced in Eq. 2.27. κ value controls the order of magnitude of adaptive step size $\mu(l)$. If the INR of the interferer approaches zero $\mu(l)$ approaches infinity and becomes unstable. Therefore, ς protects $\mu(l)$ against instability.

Substituting $\mu(l)$ instead of μ in Eq. 2.17 gives us the new Eq. 2.28, which is the weight vector for the N-LMS algorithm. The N-LMS the weight vector is defined as:

$$\mathbf{w}(l+1) = \mathbf{P}_\perp [\mathbf{w}(l) - \mu(l) \mathbf{p}(l) \mathbf{p}(l)^H \mathbf{w}(l)] + \mathbf{w}_q. \quad (2.28)$$

2.4 DMR algorithm

This section describes the Dominant Mode Rejection algorithm developed by Abraham and Owsley [2]. In later chapters the performance of the LMS techniques are compared to DMR. The DMR [10] algorithm follows its results from the MVDR weight vector obtained in the Eq. 2.8. The DMR replaces the ECM, used in MVDR, with a structured covariance matrix based on the eigendecomposition of the SCM. A structured covariance matrix assumes the eigenspace spanned by the eigenvectors is divided in the loud signal or interference subspace and the noise subspace. This makes the algorithm work only the eigenspace corresponding to the loud interferer and requiring lower degrees of freedom to represent this subspace. The SCM is obtained by averaging the outer products of L data snapshots, i.e.,

$$\mathbf{S} = (1/L) \sum_{l=1}^L \mathbf{p}(l)\mathbf{p}(l)^H. \quad (2.29)$$

The DMR weight vector is defined as:

$$\mathbf{w}_{\text{DMR}} = \frac{\mathbf{v}_m - \sum_{i=1}^D \left(\frac{g_i - s_w^2}{g_i} \right) \mathbf{e}_i \mathbf{e}_i^H \mathbf{v}_m}{\mathbf{v}_m^H \mathbf{v}_m \left(1 - \sum_{i=1}^D \left(\frac{g_i - s_w^2}{g_i} \right) \cos^2(\mathbf{e}_i, \mathbf{v}_m) \right)} \quad (2.30)$$

where the estimated noise power is defined as

$$s_w^2 = \left(\frac{L}{L-1} \right) \left(\frac{1}{N-D} \right) \sum_{n=D+1}^N g_n. \quad (2.31)$$

\mathbf{e}_i is the eigenvector associated with the largest eigenvalue and s_w^2 is the estimated noise power.

In the above algorithm the eigenvector corresponding to the largest eigenvalue is used to calculate the weight vector at each step. Since the rank of the SCM, in the presence of single interferer, is not estimated it is referred to as Fixed Rank DMR (FR-DMR). With multiple interferers at the input a need for the estimation of the eigenvectors corresponding to the interferers with highest power becomes critical. To address this situation the DMR adaptive beamformer[10], called as Estimated Rank DMR (ER-DMR) throughout the paper, is introduced.

Unlike FR-DMR, ER-DMR algorithm estimates the rank of the covariance matrix of the sensor input, in calculating the weight vector. The rank here means the number planewaves in Eq. 2.2 present in the input i.e., the dimension, D .

The estimator proposed by Nadakuditi and Edelman (N/E) [11] is used to estimate the rank of the input covariance matrix, D . Equations 2.33 and 2.32 present the N/E rank estimator equations:

$$t_d = N[(N - d) \frac{\sum_{i=d+1}^N \gamma_i^2}{(\sum_{i=d+1}^N \gamma_i)^2} - (1 + c)], \quad 0 \leq d \leq \min(N, l), \quad c = N/L \quad (2.32)$$

where γ_i sample eigenvalue of the i th eigenvector and L is the snapshot number. First the value of t_d is computed for different range of d values using Eq. 2.32. The values of t_d are substituted in Eq. 2.33:

$$\hat{D} = \min_d \left(\frac{t_d^2}{2c^2} + 2(d + 1) \right). \quad (2.33)$$

Finally, the \hat{D} value corresponding to the minimum value of the expression in the braces of Eq. 2.33 is considered to be the dimension. The ER-DMR weight vector is same as the

DMR weight vector except the number of dimensions of the signal subspace, \hat{D} is estimated:

$$\mathbf{w}_{\text{ER-DMR}}(\theta_m) = \frac{\mathbf{v}_m - \sum_{i=1}^{\hat{D}} (\mathbf{e}_i^H \mathbf{v}_m) \mathbf{e}_i}{\mathbf{v}_m^H \mathbf{v}_m - \sum_{i=1}^{\hat{D}} |(\mathbf{e}_i^H \mathbf{v}_m)|^2} \quad (2.34)$$

γ_n are the sample eigenvalues and \mathbf{e}_n are the sample eigenvectors obtained from SCM using n snapshots.

Knowing the formulation of the different algorithms used in the paper namely Frost LMS and DMR, the next step is to compare and analyze the performance of these algorithms. In the following chapters empirical results are presented to compare the performance of above two algorithms based on ND characteristic. In addition the empirical results include the cost of attaining the ND for both the algorithms in different scenarios. The cost is measured in terms of WNG. The empirical results for single interferer case are presented in chapter 3, followed by the empirical results for the multi interferer case in chapter 4.

Chapter 3: Empirical Study of the Single Interferer Case

This chapter investigates the performance of Frost LMS beamformer for a standard single interferer case. Sec. 3.1 outlines the simulation parameters used for simulations in Chapter 3. This thesis focuses only on interferers outside the mainlobe because when interferers enter the mainlobe, it is very difficult to get rid of them. Once they get close enough to the look direction, there is little that the beamformer can do. In Chapter 2 it is clear that SD weight vector is obtained by taking the expectation of the Frost LMS weight vector. Also SD assumes a known covariance structure with no uncertainty. Thus, it is of interest to evaluate the performance of SD beamformer which uses known covariance model which helps in understanding the performance of Frost LMS clearly. Sections 3.2 and 3.3 present the ND results for gradient descent algorithms such as SD and Frost LMS. Specifically, it presents empirical results for how ND varies with snapshots, step size, and INR. In addition we also investigate the effect of ND on WNG. Sec. 3.4 presents the above analysis for the Normalized-LMS (N-LMS) algorithm [12]. Finally Sec. 3.5 compares the performance of N-LMS and ER-DMR beamformers.

3.1 Simulation Parameters

The simulation parameters used in this chapter are number of sensors, $N=50$, direction of arrival of the interferer is at an angle θ corresponding to the u value of 0.06, INR= 40 dB, white noise power $\sigma_w^2 = 1$ and wavelength λ is 25. The distance between and two sensors is half of the wavelength i.e. 12.5. The stable range of step size 2.26 was reinstated in SD section of chapter 2. The challenge here is to determine maximum eigen value $(\gamma_i)_{max}$ in the upper bound of μ .

Calculating the maximum eigenvalue becomes easier by applying the Random Matrix Theory (RMT) [13] principles to decompose ECM Σ into eigenvectors and eigenvalues. It is straightforward to demonstrate that the interferer replica vector is an eigenvector of the covariance matrix for the single interferer case. For a standard single interferer case the number of dimensions D is 1. Therefore, ECM for a standard single interferer case becomes:

$$\Sigma = \mathcal{E} \{ \mathbf{p}\mathbf{p}^H \} = \sigma_1^2 \mathbf{v}_1 \mathbf{v}_1^H + \sigma_w^2 \mathbf{I} \quad (3.1)$$

where σ_1^2 is the power of the single interferer and \mathbf{v}_1 is the replica vector of the single interferer. Multiplying Eq. 3.1 by the \mathbf{v}_1 , replica vector of interferer:

$$\Sigma \mathbf{v}_1 = \sigma_1^2 \mathbf{v}_1 \mathbf{v}_1^H \mathbf{v}_1 + \sigma_w^2 \mathbf{v}_1 = (N\sigma_1^2 + \sigma_w^2) \mathbf{v}_1, \quad (3.2)$$

where $\mathbf{v}_1^H \mathbf{v}_1 = \|\mathbf{v}_1\|^2 = N$ in Eq. 3.2. By definition eigenvector of a covariance matrix, which is non-zero vector \mathbf{v}_1 , when multiplied by the covariance matrix Σ yields the same result as when some scalar multiplies \mathbf{v}_1 . The scalar is called the eigenvalue which is $N\sigma_1^2 + \sigma_w^2$ in this case. The other $N - 1$ eigenvectors correspond to the noise subspace. Thus, $N\sigma_1^2 + \sigma_w^2$ is the largest eigenvalue and the corresponding eigenvector is \mathbf{v}_1 forms the signal or interferer subspace. Eq. 3.3 provides the mathematical calculation of maximum eigenvalue for the standard single interferer case.

$$\max(\gamma_i) = N\sigma_i^2 + \sigma_w^2 = 10000 * 50 + 1 = 500,001 \quad (3.3)$$

where σ_i^2 is 10000, for a standard case with INR = 40 dB. Thus, the maximum limit on μ for the standard case is $2/500,001 = 0.000004$.

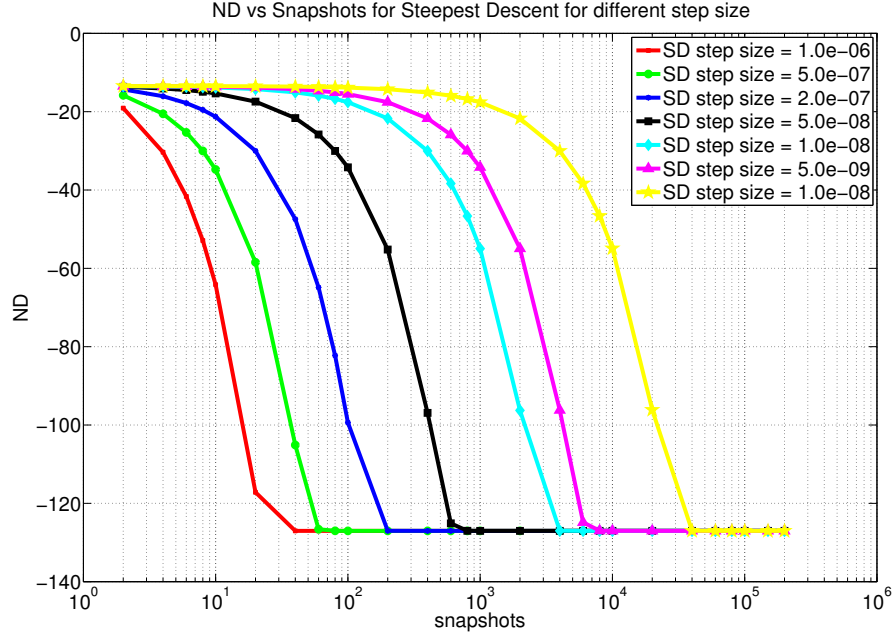


Figure 3.1: ND vs. snapshots for SD algorithm. Each curve uses different μ values. All the curves are considered with 40 dB INR at the input

3.2 Analysis of Steepest Descent Beamformer

This section analyzes the performance of SD beamformer. The simulation in Fig. 3.1 shows the variation of ND against snapshots for different choice of step size in SD algorithm. The first observation made from the results in Fig. 3.1 is that the SD algorithm is reaching a ND of -127 dB, the optimum ND attained by the MVDR beamformer. The convergence to the optimum ND for SD is possible because the SD descent beamformer uses a known covariance model, which means there is no noise in the estimation of covariance matrix. The second observation is the speed of convergence of the SD algorithm is decreasing with decrease in μ . Lower step sizes lead to slower convergence. Larger step sizes greater than or equal to the upper bound on μ cause the algorithm to become unstable. Thus, the upper bound on the μ governs the performance of the SD algorithm.

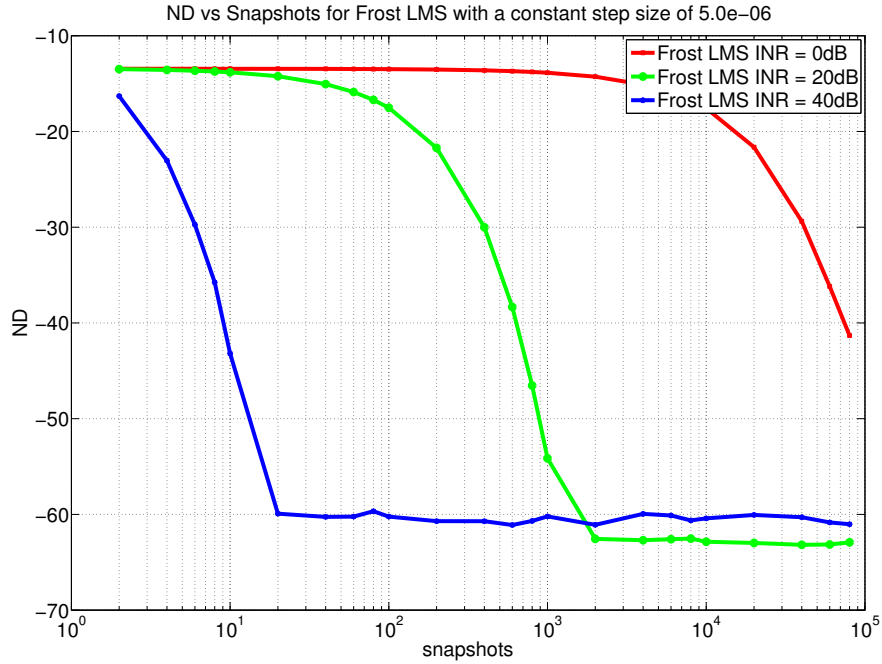


Figure 3.2: ND vs. snapshots for Frost LMS algorithm. Different curves represent different INR levels namely 40 dB, 20 dB, 0 dB. All the curves are considered with a constant μ value of 0.000001

3.3 Analysis of Frost LMS Beamformer

3.3.1 ND performance of Frost LMS beamformer

Understanding the effect of μ on simple gradient descent algorithm i.e SD, the next step is to replace the ECM in SD with an instantaneous estimate which leads to the Frost LMS algorithm. The empirical results include the variation of ND vs snapshots for the 3 different INR levels namely 0 dB, 20 dB and 40 dB for Frost LMS. Section 3.3.1 presents the ND variation against snapshots and step size for Frost LMS beamformer. Section 3.3.2 analyzes the WNG performance of Frost LMS beamformer.

Frost LMS algorithm uses an instantaneous estimate unlike SD which uses a ECM. Thus, the same bound on the μ used for SD can be applied Frost LMS as well. The maximum bound on the μ can be obtained for all the INRs by just changing the σ_i^2 value in Eq. 3.3. The values of σ_i^2 are 1,100 and 10000 for 0 dB, 20 dB and 40 dB respectively and the maximum bounds on μ are 0.04, 0.0004 and 0.000004. To simplify the understanding of Frost LMS a constant μ is used for different INR levels in the simulation performed in Fig. 3.2.

Fig. 3.2 compares the performance of Frost LMS for three different INR levels namely 0 dB, 20 dB, 40 dB. The ND calculated at each snapshot is an average value of 300 Monte Carlo trials. The maximum bound of μ for 0 dB and 40 dB INR are 0.04 and 0.000004 respectively. Thus, a constant μ value of 0.000001 is chosen for simulation purposes such that the algorithm remains stable for all the INR levels.

Fig. 3.2 shows that the ND is reaching a limiting value for a specific μ value which can be termed as Steady State Notch Depth (SSND). Although the Frost LMS attains the SSND, its value is -61 dB different from the optimum ND of -127 dB for MVDR beamformer for a constant step size of 1.0e-06. The blue line representing the 40 dB INR convergence the fastest than other two INR levels namely 0 dB and 20 dB. On the other hand, the red line representing the 0 dB INR convergence the slowest. In fact, an excess of 80000 snapshots are required to observe this SSND level for the 0 dB INR case. The take away point is that with a constant μ , lower the INR slower is the convergence.

As a next step a different stable μ is chosen for all the three INRs 0 dB, 20 dB and 40 dB. Here, the μ values chosen are one order of magnitude less than the maximum eigenvalue calculated for each INR level. Fig. 3.3 compares the ND vs snapshots for three different INRs. The values of SSND are -33 dB, -53 dB and -70 dB for 0 dB, 20 dB and 40 dB INRs respectively, while their corresponding optimum ND values are -47 dB, -87 dB, -127 dB. The difference in ND between SSND and optimum ND are 14 dB, 34 dB and 57 dB for

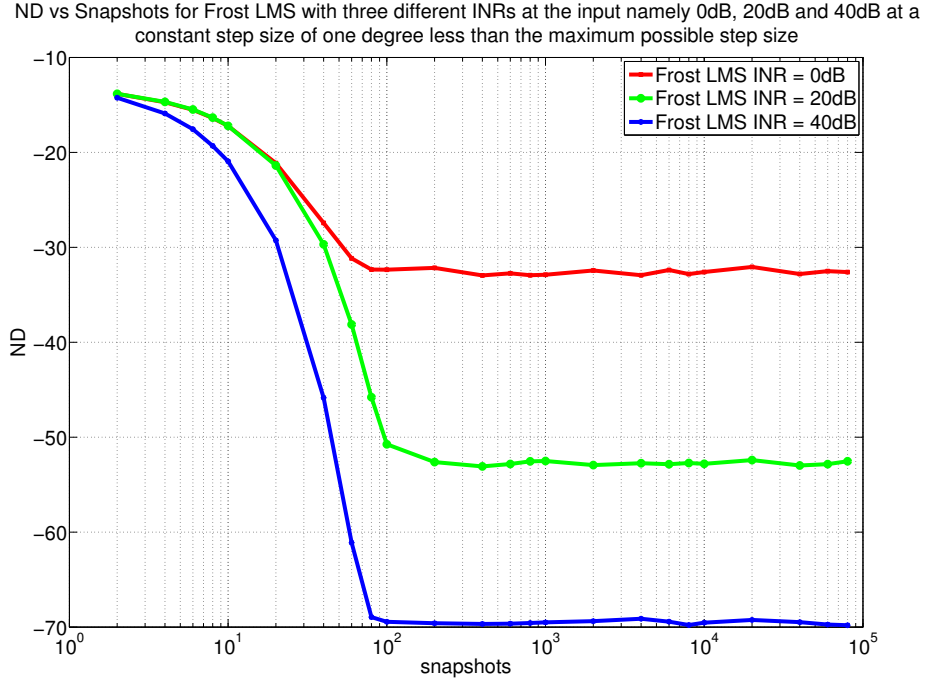


Figure 3.3: ND vs. snapshots for Frost LMS algorithm for a standard case with three different INR levels namely 0 dB, 20 dB and 40 dB. A one degree less than the maximum possible step size is used as μ for simulation purposes.

0 dB, 20 dB and 40 dB INRs respectively. This difference exists here because of the fact there is an additional noise introduced at the output of the beamformer due to the use of $\mathbf{p}\mathbf{p}^H$ instead of the ensemble covariance matrix $\mathbf{\Sigma}$ in the weight update.

Fig. 3.4 illustrates the dependence of SSND level on the value of μ , for a 40 dB INR case. The figure clearly shows that SSND decreases as μ decreases. The level of SSND is attained by a μ with order of 6 ($1 * 10^{-6}$), is -60 dB while it is -90 dB for a μ of order 9 ($1 * 10^{-9}$). At the same time decrease in μ leads to slower rate of convergence. The number of snapshots required to converge for the μ of order 9 is 10000 while it is 100 for μ of order 6. Thus, the step size governs both the speed of convergence and the SSND attained. In addition, SSND is dependent on both INR as well as μ from Figures 3.2 and 3.3. From Fig. 3.4 it is clear that to attain the optimum ND the algorithm requires a very low μ . Number of

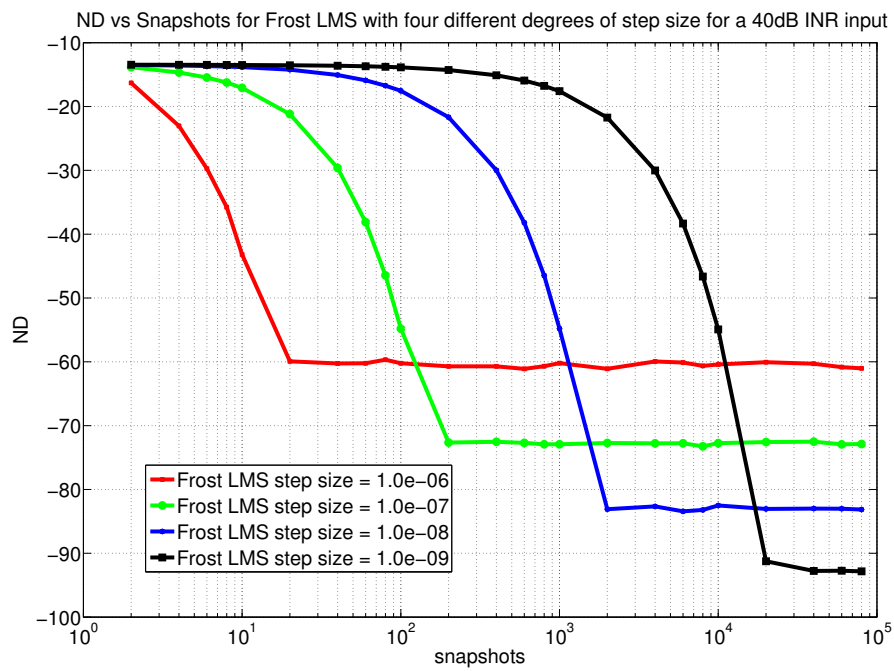


Figure 3.4: ND vs. snapshots for Frost LMS algorithm. Different curves represent different μ values used. All the curves are assume a 40 dB INR interferer

snapshots increases as μ decreases. Therefore, prediction is the best way to decide the μ value required to attain the optimum ND. This can be achieved by curve fitting the results of SSND vs μ for 40 dB INR, which is the case of interest.

Evaluating the trend of SSND based on μ is the next task. In order observe this trend it is beneficial to plot the variation of ND with μ for the 0 dB INR case. This is because for 0 dB INR, the number of snapshots required for Frost LMS to achieve the MVDR performance is smaller than for 40 dB INR case. In addition another goal is to determine that the SSND vs μ trend are similar for all INRs.

First the SSND values are recorded for 300 Monte Carlo trials for the required set of step sizes and INRs. Fig. 3.5 depicts the distribution of the mean of 300 values of SSND at each μ with 0 dB INR input. It is clear that there are three different regions for the curve. First region is where the range of values of μ for which ND is unstable. Second region is where the ND follows an approximately linear trend with decrease in μ . Third region is where the range of values of μ for which the ND remains at a constant SSND for a particular INR. It can be observed clearly that as the μ decreases, SSND decreases, which implies the number of snapshots required increases. The starting point of μ of the first region of the curve, for 0 dB and 40 dB INRs 0.04 and 0.000004 respectively. In addition, the SSND achieved is different for different INRs, as presented in Fig. 3.3 which proves that the distribution of the third region of the curve varies based on the INRs. It implies that the third region is unique for different interferers. Thus, predicting the linear trend or the second region of this curve for different INRs becomes important because it helps in predicting the μ and number of snapshots required to attain a particular SSND.

The point of interest is to see if the linear trend followed by the SSND vs μ curve follows the same trend irrespective of the INR at the input. Therefore, moving forward the distribution of ND vs μ are presented for different INRs considering on the linear section of the curve in Fig. 3.5 for different INRs. Fig. 3.6 depicts the SSND vs μ plot for different

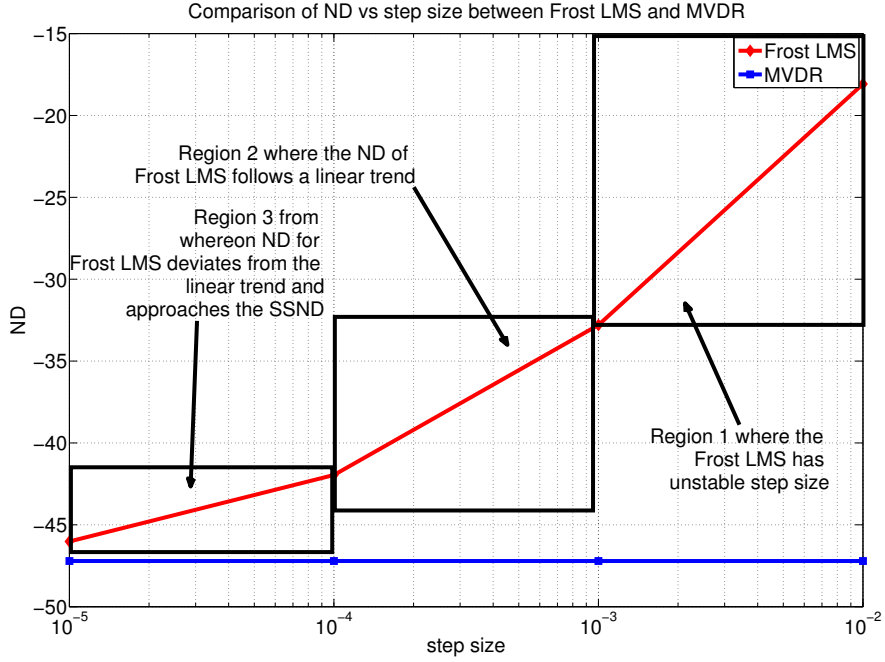


Figure 3.5: SSND vs. μ comparison between Frost LMS and MVDR algorithms.

INRs namely 40 dB, 37 dB and 20 dB. At each step size 1500 values of SSND are used to calculate the distribution of SSND. In addition, error bars are also indicated to see if there are any deviation from the linear trend. The line fit for each INR is obtained by taking the mean of the 1500 values of SSND at each μ . The higher and lower ends of the error bars correspond to 10 and 80 percent of the Cumulative Distribution Function (CDF) of the SSND at each μ , for a particular INR. For SSND values corresponding to μ 's namely 1.0e-007, 2.0e-007 and 3.0e-007 are shifted towards left and right, for 37 dB and 20 dB respectively, with no change for 40 dB INR. This shift is introduced to differentiate the distribution of SSND as well as the error bars for different INRs. The mean of SSND values for different INRs follow the same trend irrespective of the INR at the input. First implication is that the trend of the mean of SSND is same for all the three INRs. This brings down to a conclusion that the mean of SSND varies linearly with μ irrespective of the INR at the input. Secondly, the 20 and 80 percentile values of the error bars are also

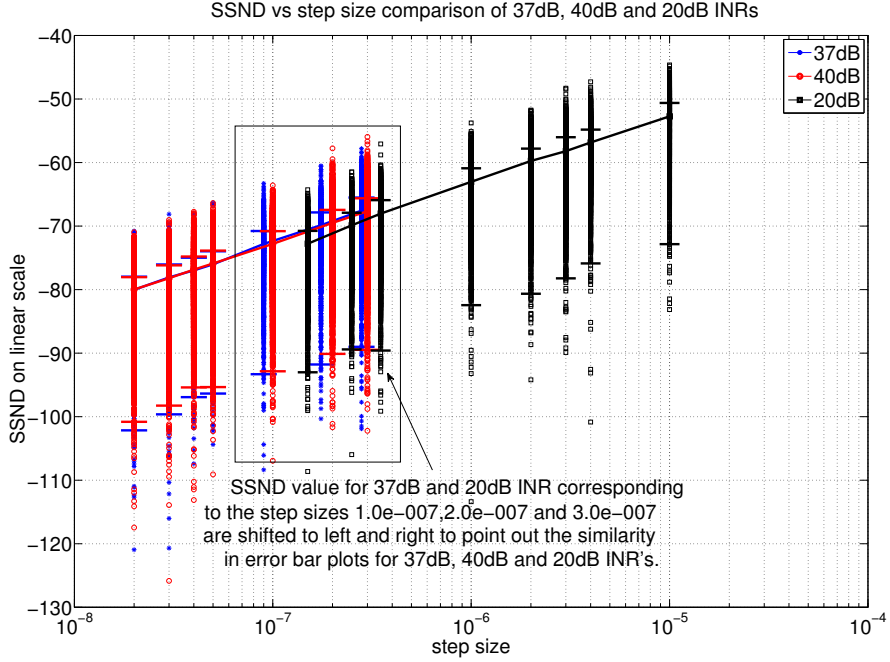


Figure 3.6: SSND vs μ comparison between 40 dB, 37 dB and 20 dB INRs.

linearly decreasing as step size increasing.

In order to validate and confirm the above observations comparison of SSND vs step size is provided for 20 dB and 10 dB, 10 dB and 2 dB in Fig. 3.7, 3.8 respectively. In each of the comparison's even though the step size's are different, the observations made for Fig. 3.6 are still valid. Thus, the linear trend could be generalized for all INRs which facilitates to estimate the μ and number of snapshots required to achieve a particular SSND irrespective of the INR.

Following the above observation the prediction curve on the SSND vs μ using 40 dB INR is presented in Fig. 3.9. The red line depicts variation of SSND against μ for and the blue line is the prediction curve attained by linear curve fitting method. Following from the previous discussion, the level of the SSND is decreasing in the direction of decreased μ , which is clearly observed in Fig. 3.9. It is approximately following a linear trend. Eq. 3.4

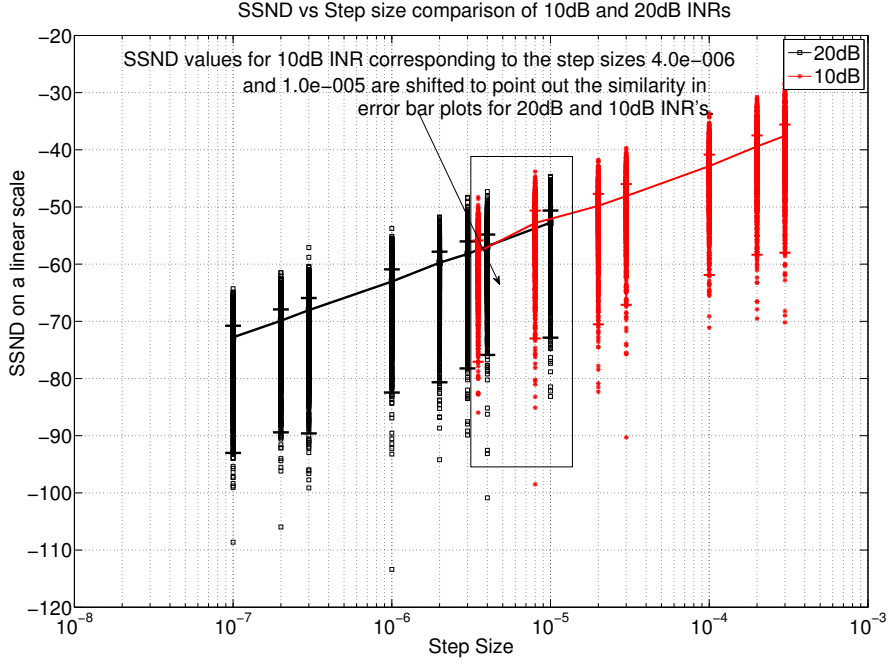


Figure 3.7: SSND vs μ comparison between 20 dB and 10 dB INRs.

is the polynomial fit for the red curve and is calculated such that it is the best fit in least-squares sense. The value 10.1846 in Eq. 3.4 indicates the slope which implies that the level of SSND drops down by 10.1846 dB for every one degree reduction in μ .

$$ND = 10.1846\mu - 1.6521 \quad (3.4)$$

3.3.2 White Noise Gain for Frost LMS beamformer

In Figures 3.2 and 3.4, it is clear that the Frost LMS algorithm attains the ND at some cost. This cost is measured in terms of WNG. It is more intuitive if the comparison is made between MVDR, CBF and Frost LMS. This is because it shows the measure of WNG that is paid for using an instantaneous estimate in Frost LMS versus using an ECM in MVDR. Fig. 3.10, 3.11 and 3.12 depict the variation of WNG against snapshots for three different INRs namely 0 dB, 20 dB and 40 dB. In all the three cases the WNG for CBF is 17 dB

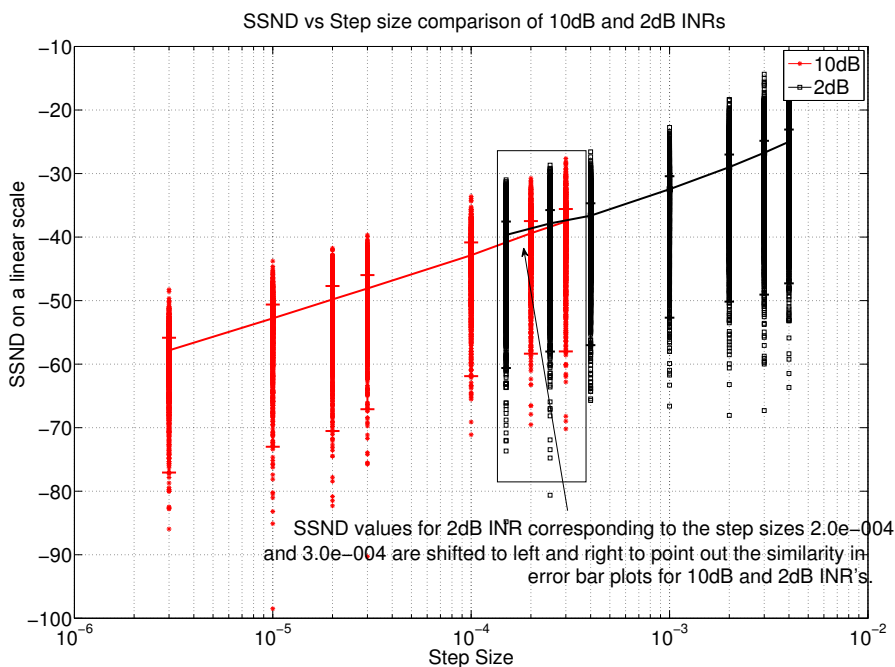


Figure 3.8: SSND vs μ comparison between 10 dB and 2 dB INRs.

which is the maximum WNG possible. For MVDR and SD, WNG is 16.72 dB for all three INRs. On the other hand, for Frost LMS algorithm the speed at which the WNG reaches the sub optimum WNG level of MVDR beamformer depends on the μ . Except for the case of 0 dB INR when the μ is 0.01, which is close to the maximum μ allowed i.e. 0.04, the WNG falls rapidly by 3 dB. This is because of the instability in the beamformer due to a value of μ larger than the allowable value. This instability effect could be clearly observed from the ND curve for 0 dB INR in Fig. 3.13.

The conclusion made here is that the speed of convergence and level of SSND attained by the Frost LMS algorithm for the case of the constant μ depends on the μ and INR. Lower the μ slower is the convergence and deeper the notch. The upper bound on μ , which decides the stability of the algorithm, is based on the INR while the lower bound is based on the requirement of the speed of convergence. The cost of placing the notch is measured by using the characteristic called the WNG. For the WNG to reach the sub optimal WNG

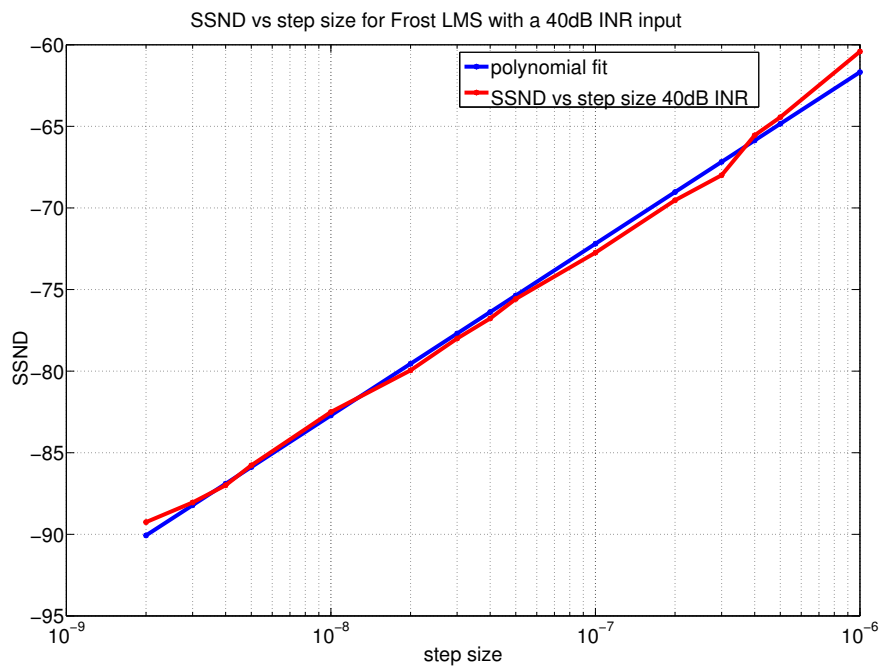


Figure 3.9: Curve fitting of SSND vs. μ with ND values obtained by using different INRs at the input. A least squares fit method is used to fit the curve.

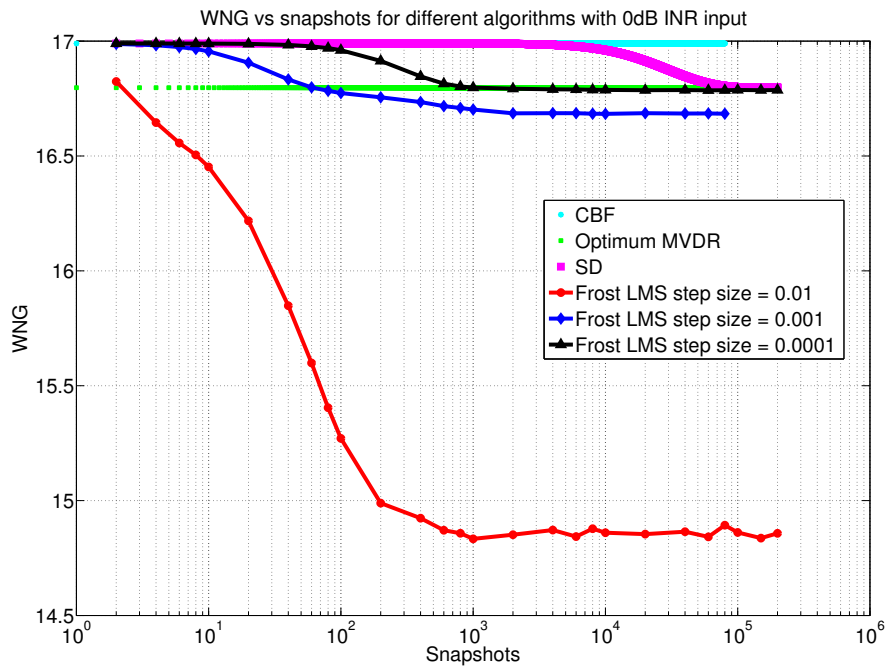


Figure 3.10: Comparison of WNG of CBF, MVDR, SD and Frost LMS (with three different μ 's namely 0.01, 0.001 and 0.0001) for a 0 dB INR

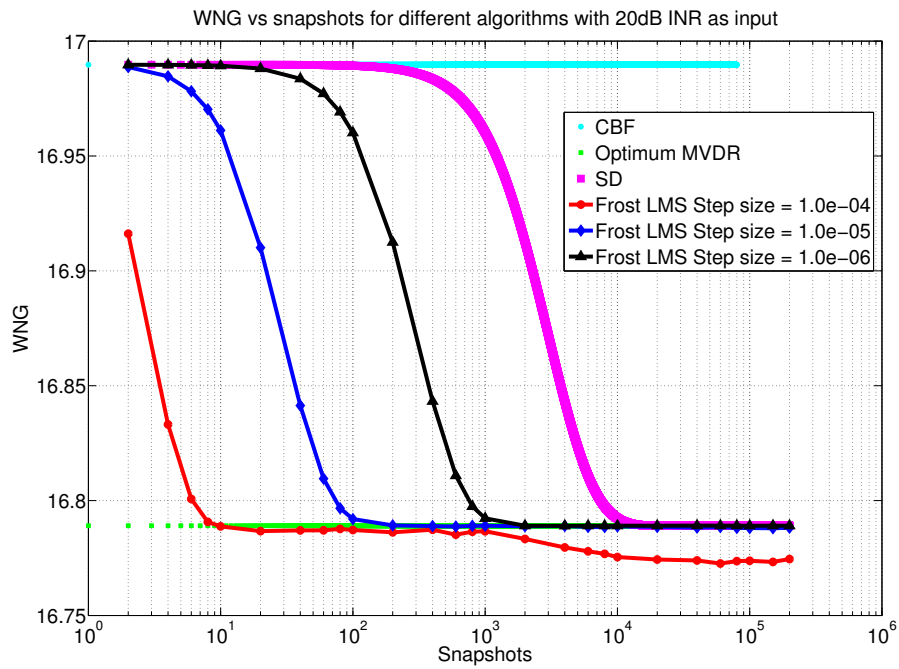


Figure 3.11: Comparison of WNG of CBF, MVDR, SD and Frost LMS (with three different μ 's namely 0.0001, 0.00001 and 0.000001) for a 20 dB INR

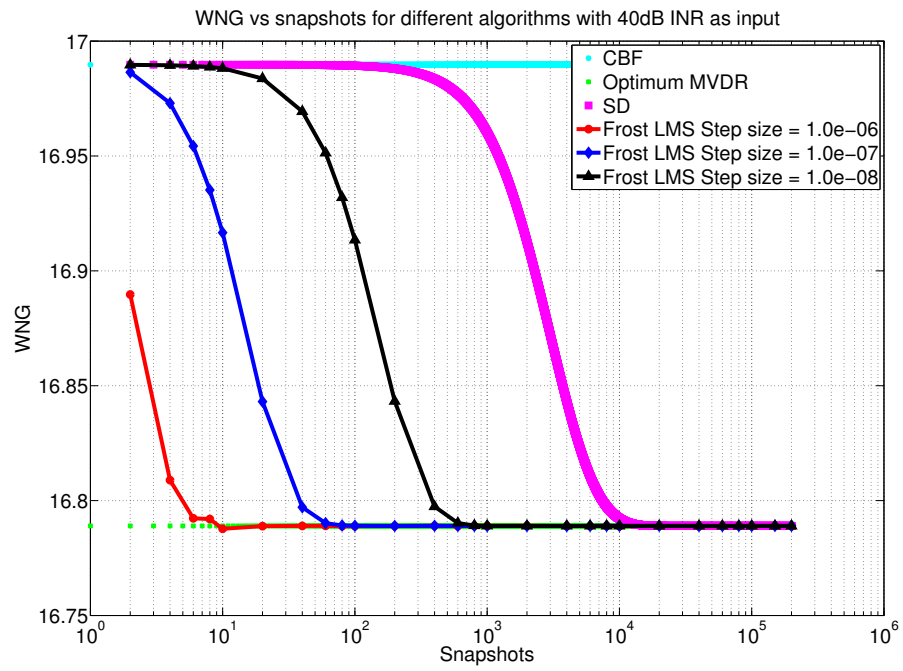


Figure 3.12: Comparison of WNG of CBF, MVDR, SD and Frost LMS (with three different μ 's namely 0.000001, 0.0000001 and 0.00000001) for a 40 dB INR

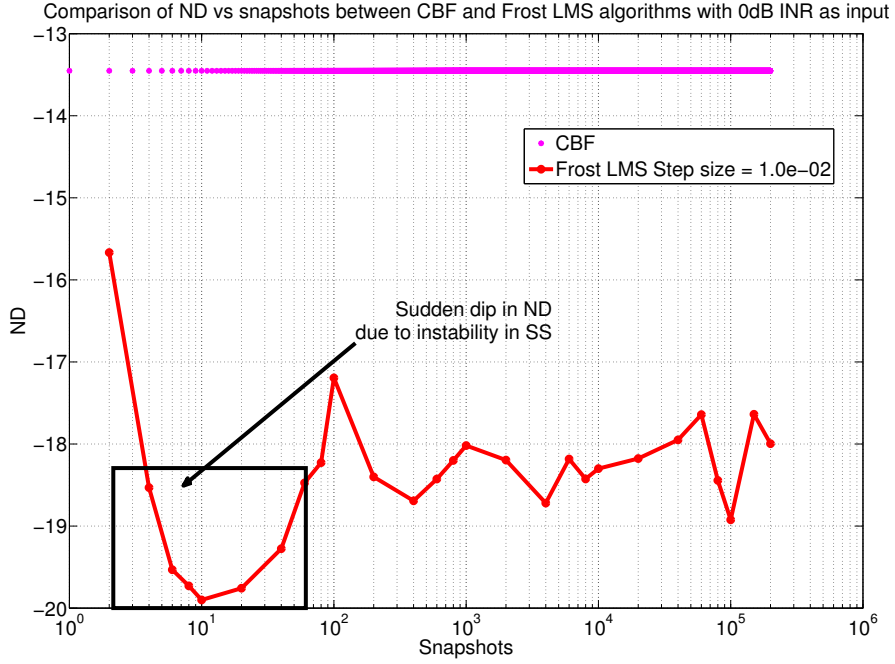


Figure 3.13: Comparison of ND of CBF and Frost LMS (with μ of 0.01) for 0 dB INR

of MVDR, a μ should be chosen in such a way that the algorithm does not become unstable. Understanding the characteristics of Frost LMS under constant μ helps in migrating towards the N-LMS case. In Sec. 3.4 we investigate the empirical results of N-LMS i.e. ND and WNG vs snapshots for different INRs. This analysis forms the basis for the comparison of these results with FR-DMR in 3.5.

3.4 Analysis of N-LMS beamformer

The characteristics of ND and WNG observed for Frost LMS for the case of fixed μ , in the previous section, are extended to N-LMS. The $\mu(l)$ term in N-LMS algorithm as two constants namely κ and ζ in the numerator and denominator respectively are introduced in Eq. 2.27, $\mu(l) = \frac{\kappa}{\zeta + \mathbf{p}(l)^H \mathbf{p}(l)}$. Understanding the effect of these two constants on the behavior of N-LMS algorithm is the first step towards analyzing N-LMS performance.

Instability in the beamformer is observed when the term $\mathbf{p}(l)^H \mathbf{p}(l)$ in the denominator becomes zero. For example, consider ς as 1 and input INRs of -20 dB. The expected value of the denominator term of 2.27 i.e. $\mathbf{p}(l)^H \mathbf{p}(l)$ becomes 0.5 which increases the effective value of $\mu(l)$ which leads to instability of the LMS algorithm. To protect the beamformer against this problem the parameter ς is used in the denominator. The importance of the second parameter in the μ , κ , is presented in the later part of this section. As cited in [3] the range of κ is between 0 and 2, while ς should be greater than zero.

Fig. 3.14 present shows a simulation of ND vs snapshots for N-LMS algorithm for three different INRs 0 dB, 20 dB and 40 dB. In all the cases the parameter $\varsigma = 1$, to make sure that the beamformer never goes unstable. The value of κ is chosen to be one so that it doesn't change the order of magnitude of adaptive step size $\mu(l)$ which implies that it doesn't effect the convergence of the N-LMS weight vector. The first observation is that the SSND level is increasing with increase in INR. SSND levels are -20 dB, -32 dB and -50 dB approximately for 0 dB, 20 dB and 40 dB INRs. The second observation is that the speed of convergence of N-LMS to the SSND level adaptively changes based on the INR of the interferer, unlike the Frost LMS in which it could be controlled by the constant step size of choice. By comparison of the Fig. 3.2 and Fig. 3.14 the first noticeable difference between Frost LMS and N-LMS is that SSND level attained is different even if the same INR is used for both the algorithms. This is because of the above mentioned fact that in N-LMS $\mu(l)$ is dependent of instantaneous input, while in Frost LMS case step size is constant. For example approximate SSND level attained for 40 dB INR for Frost LMS and N-LMS algorithms are -60 dB and -50 dB respectively from Figures 3.4 and 3.14. The second difference follows from the fact that there is a variance associated with the SSND level of N-LMS, which is very negligible for Frost LMS. This is because of the $\mu(l)$ is varying with change in input. The histogram comparison of the SSND level in Fig. 3.15 makes this fact clear.

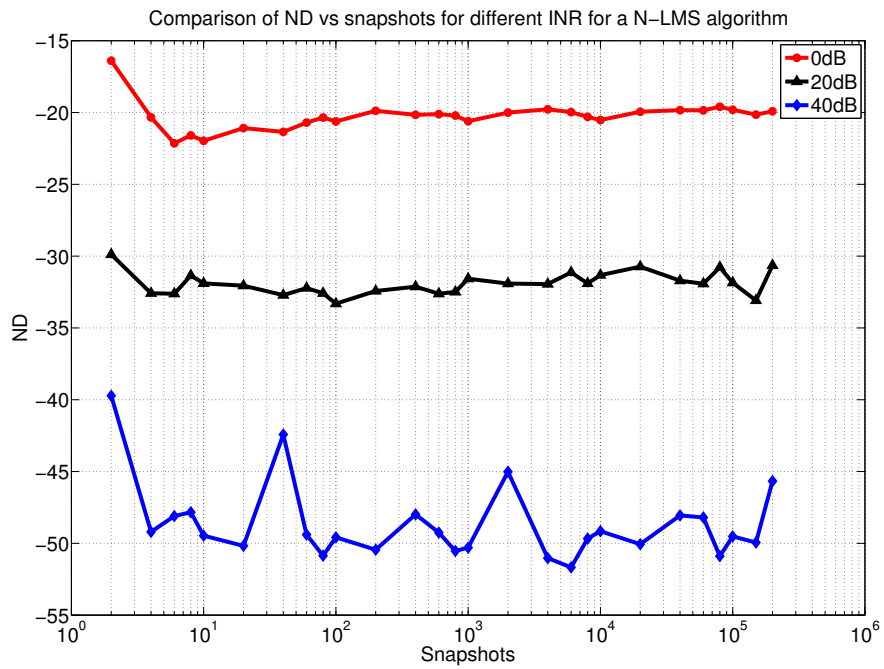


Figure 3.14: ND vs. snapshots for a N- LMS algorithm, with a variable μ , for different INRs namely 40 dB, 20 dB, 0 dB. Here the values of $\kappa = 1$ and $\varsigma = 1$

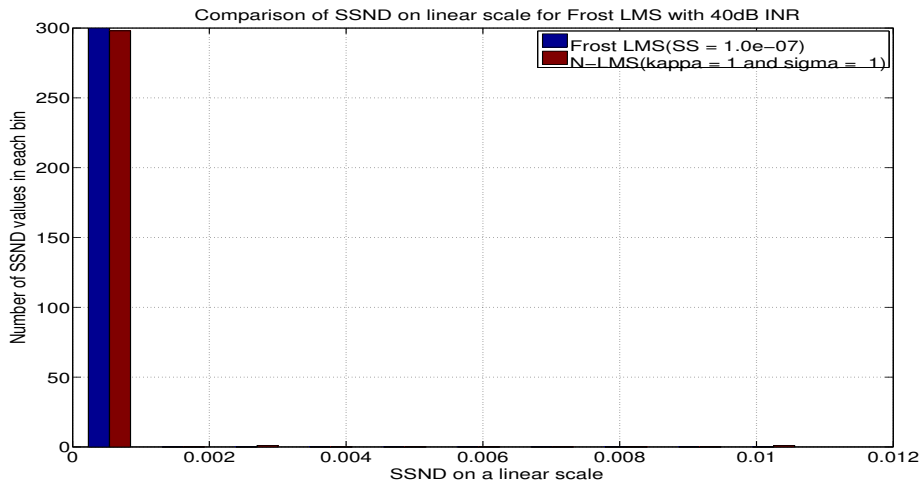
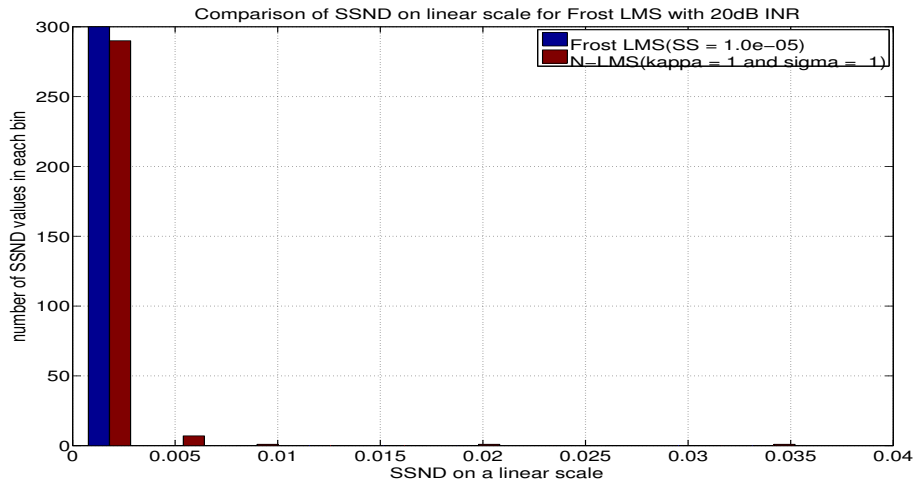
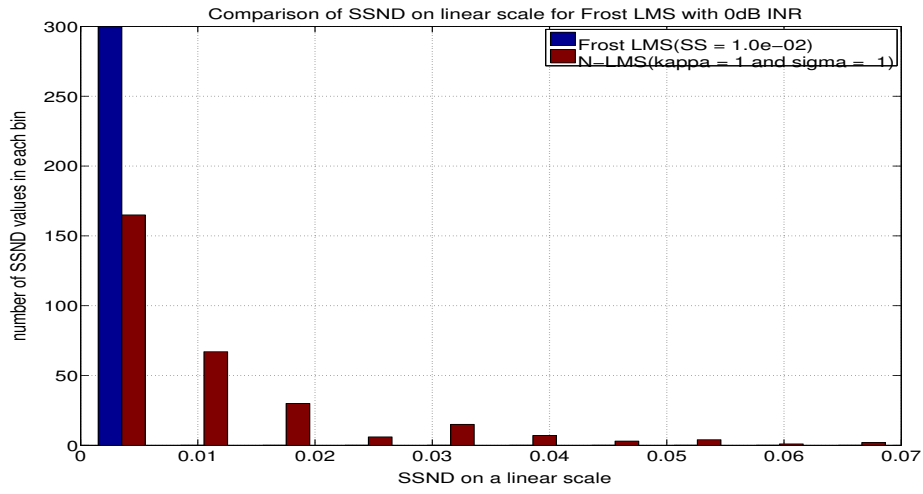


Figure 3.15: Comparing the mean and variance of SSND of Frost LMS and N-LMS at 10000th.

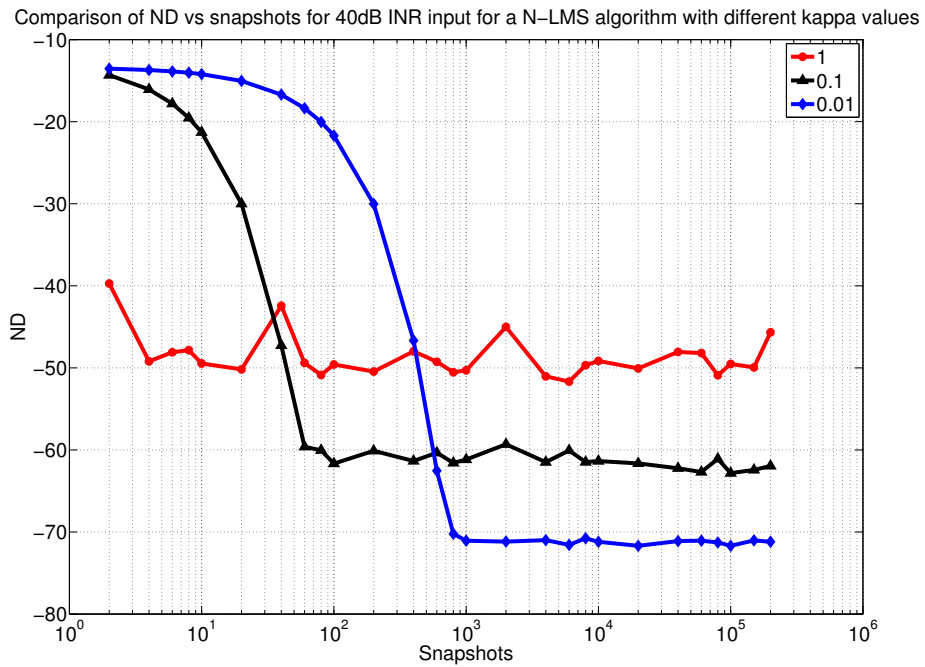


Figure 3.16: ND vs. snapshots for a N-LMS algorithm, with a variable μ , only with 40 dB INR as input to the beamformer. Here the three curves represent three different κ values namely 1,0.1,0.01

The three histograms in Fig. 3.15 present the variation of SSND for 300 Monte Carlo trials at the 10000th snapshot for three different INR levels 0 dB, 20 dB and 40 dB. The histograms are considered on a linear scale of ND in order to measure the variance of ND. The μ values used for Frost LMS are one degree less than the maximum μ possible for each INR. The variance of the SSND around its mean is decreasing with increase in INR for the N-LMS algorithm, while there is negligible variance in the Frost LMS case. This is clearly shown by the bin count number for the highest bin for both Frost LMS and N-LMS. As shown in Fig. 3.15 the highest bin count is 300 for all three INRs for Frost LMS, while it is 165, 290 and 298 for N-LMS for 0 dB, 20 dB and 40 dB INRs. Implies that for Frost LMS bin count number, i.e. mean is 300 and is equal to the number of Monte Carlo trials. On the other hand, mean bit count number is increasing from 165 to 298 by increasing the INR from 0 dB to 40 dB. Thus, the variance of ND, at the SSND level, is decreasing with increase in INR for N-LMS. Moving forward understanding the behavior N-LMS for different κ values will be interesting.

Fig. 3.16 presents the ND versus snapshot results for a 40 dB INR case, with different κ values 1, 0.1 and 0.01. Firstly, it could be observed that as the order of κ is increasing the SSND level is dropping. Secondly, there is sudden jump in the SSND level with a change in κ from 0.1 to 0.01. This shows that initializing the κ value to 0.01 makes the SSND level drop so rapidly because the term in the denominator of μ becomes negligible. Implies that the SSND level attained will be dependent solely on κ value rather than by the input INR term in the denominator. This can be observed clearly that there is a linear trend observed between the SSND level of N-LMS with $\kappa = 0.05$ and Frost LMS SSND with $\mu = 5.0e-07$ in Fig. 3.17

The first conclusion to be made is that the SSND level of the N-LMS algorithm depends on the INR at the input. Secondly, this level can be further decreased by the decreasing the value of κ . However, care should be taken in choosing κ such that it does not reduce to the extent wherein, the instantaneous $\mu(l)$ depends only on κ and does not depend on INR.

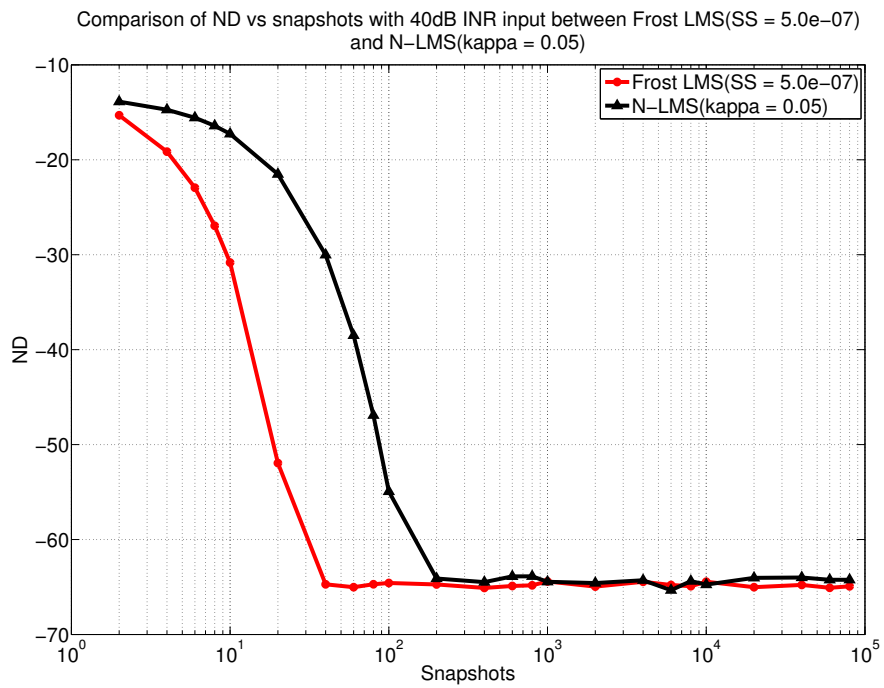


Figure 3.17: Comparison of ND vs snapshots of Frost LMS ($\mu = 5.0e-07$) and N-LMS ($\kappa = 0.05$) with 40 dB INR at the input

In the next section 3.5, the empirical results obtained for N-LMS algorithm are compared with the Estimated Rank DMR (ER-DMR) [10] algorithm results.

3.5 Comparison of LMS and DMR beamformers

ER-DMR involves estimating the rank of the covariance matrix. The rank estimated from the covariance matrix decides the number of eigenvectors to be used to compute the weight vectors at l^{th} snapshot according to the Eq. 2.34. This sets a platform to make a fair comparison with N-LMS with adaptive μ , where both algorithms are adaptive with respect to input.

It is necessary to verify the performance of the ER-DMR algorithm in estimating the correct rank from the SCM. Figures 3.18 and 3.19 present the variation of ND vs snapshots FR-DMR and ER-DMR for -10 dB INR and 40 dB INR cases respectively. In both the figures the ER-DMR is following the same trend as FR-DMR in converging to a ND, for both the INR cases. Although, the ER-DMR fails to estimate the rank correctly for snapshots less than 4, leading to unfavorable ND for the -10 dB INR case, it eventually converges with the FR-DMR curve after 20 snapshots. This phenomenon is due to the insufficient number of snapshots available at the input to estimate the rank. This insufficiency in number of snapshots is measured by the parameter c in Eq. 2.32 which is the ratio of number of sensors to number of snapshots as defined in [4].

Moving forward the comparison of empirical results for N-LMS and ER-DMR are presented. Fig. 3.20 compares the N-LMS and ER-DMR algorithm's performance based on the ND against number of snapshots. Clearly, the ER-DMR beamformer places a deeper notch when compared to the N-LMS. ER-DMR achieves an SSND of -70 dB with only 20 snapshots, whereas N-LMS takes 800 snapshots to achieve the same result.. As discussed in the previous section 3.4 reducing the value of κ less than 0.01, for the 40 dB INR case, there is risk that SSND level attained becomes independent of INR like that of the constant

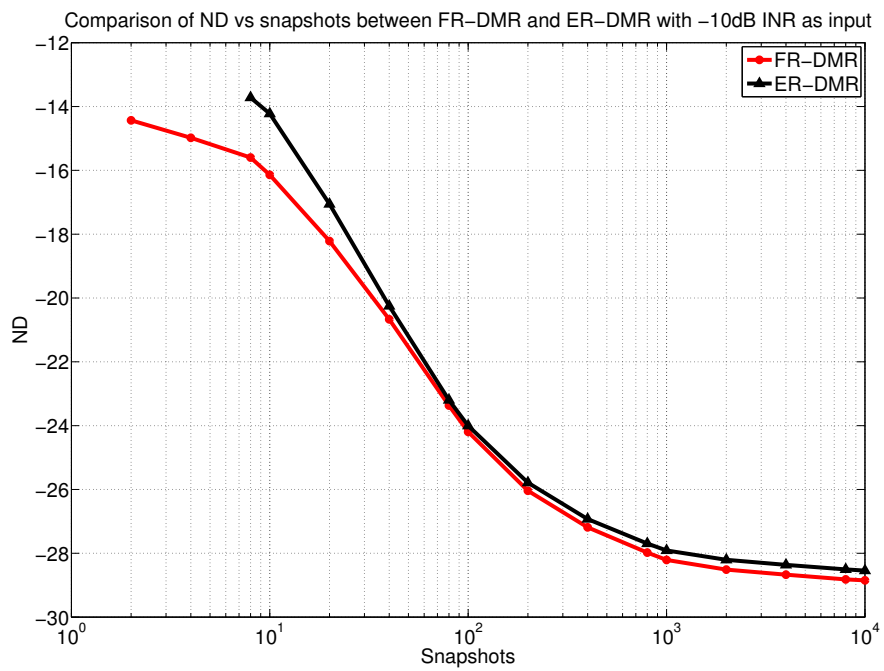


Figure 3.18: ND vs. snapshots comparison of FR-DMR and ER-DMR. The input to the beamformer is a -10 dB interferer and white noise.

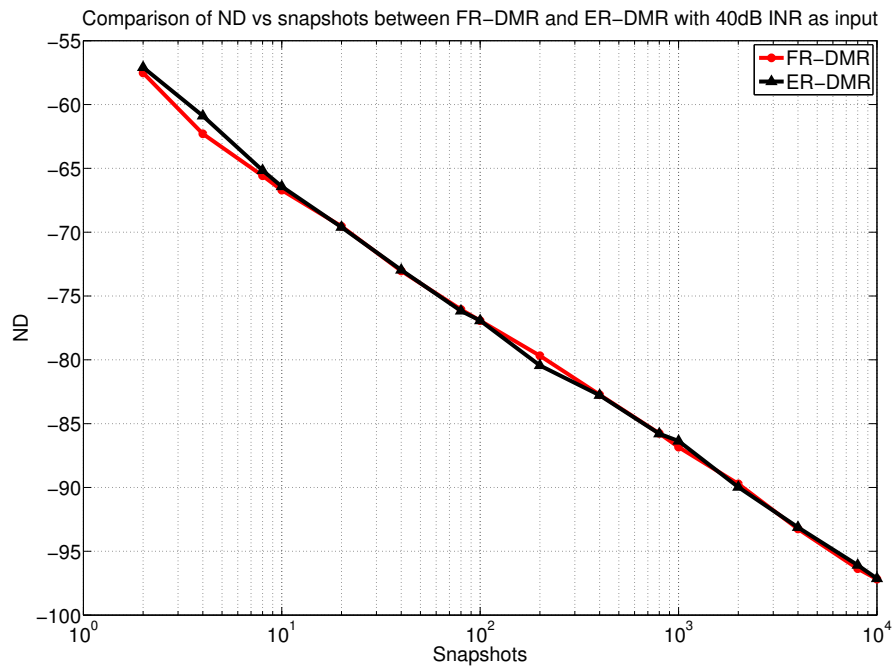


Figure 3.19: ND vs. snapshots comparison of FR-DMR and ER-DMR. The input to the beamformer is a 40 dB interferer and white noise.

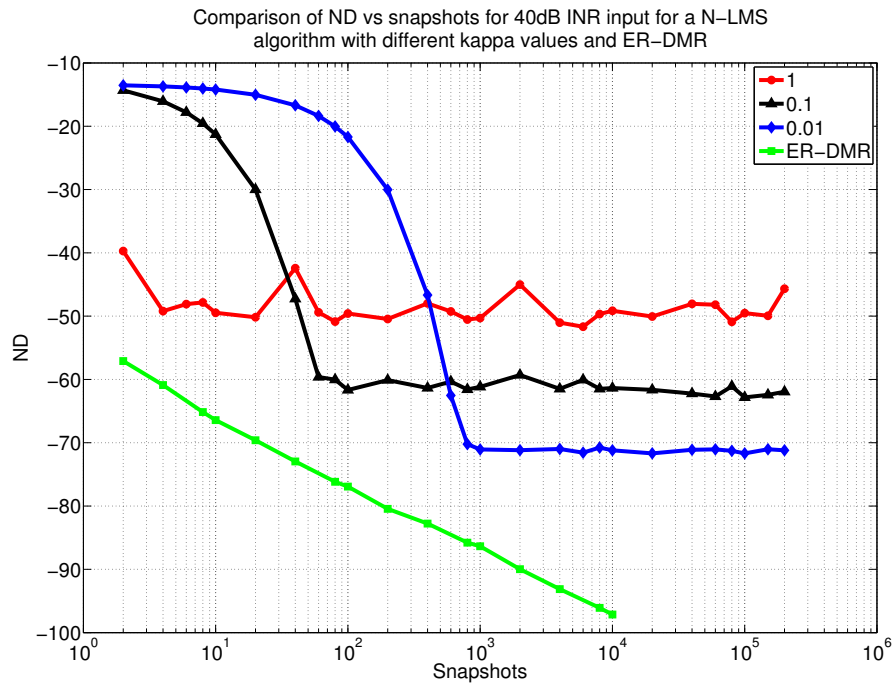


Figure 3.20: ND vs. snapshots comparison of N-LMS (variable μ) and ER-DMR (with rank estimation). The input to the beamformer is a 40 dB interferer. The N-LMS is considered with three different κ values namely 1, 0.1, 0.01

μ case. Therefore, there is a limitation on the SSND level attained by the N-LMS which is not the case for ER-DMR. In ER-DMR ND decreases with increase in the number of snapshots and there is no SSND as such for ER-DMR.

ER-DMR performance is better than N-LMS for 40 dB INR case for all κ values possible. Although both the algorithms don't reach the optimum performance attained by the MVDR algorithm with a ND of -127 dB, even with 100,000 snapshots. In addition to ND, other factor to be considered while choosing from these two algorithms is the computational complexity. Computational complexity becomes a very dominant factor in time sensitive programs and is analyzed in chapter 4. The number of computations required for N-LMS is lesser than the ER-DMR, since the eigendecomposition of eigenvalues and eigenvectors from the covariance matrix itself takes lot of computations, which is just a part of the entire algorithm.

Extending the WNG comparison presented in Fig. 3.12 for N-LMS and ER-DMR is the next step in order to understand the cost of placing the notch for both the algorithms. Fig. 3.21 compares the WNG as a function of snapshots for N-LMS and ER-DMR. The maximum WNG that could be attained is 17 dB which is for a CBF beamformer with $N = 50$. Therefore, both N-LMS and ER-DMR WNG are less than 17 dB, which is the cost for placing the notch. However, this cost varies for both the algorithms. The two observations that could be made from the Fig. 3.21 are as follows. Firstly, the ER-DMR algorithm WNG is attaining a threshold level of 16.79 dB after certain number of snapshots. Secondly, although the N-LMS WNG is reaching the threshold level of 16.79 dB faster than ER-DMR, the WNG performance is degrading after 1000 snapshots and then settling down after 100,000 snapshots. This behavior is true for all the three κ values of 1, 0.1 and 0.01.

Further probing lead to the comparison of N-LMS for different INR levels, which proved that a similar trend is followed by all the three different INRs namely 0 dB, 20 dB and 40 dB. Fig. 3.22 presents this observation.

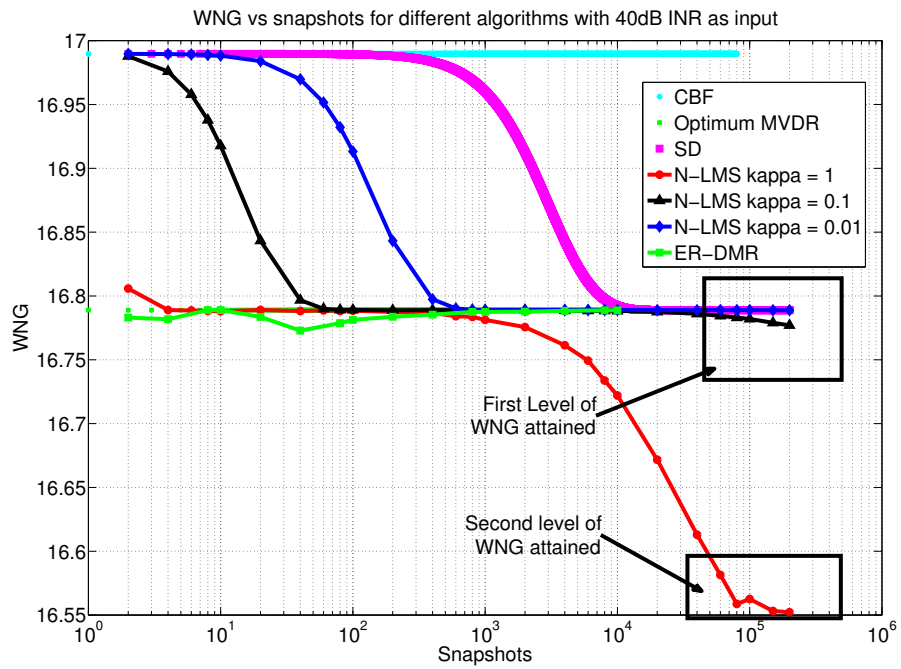


Figure 3.21: WNG comparison of N-LMS and ER-DMR for the standard single interferer case with 40 dB INR as input.

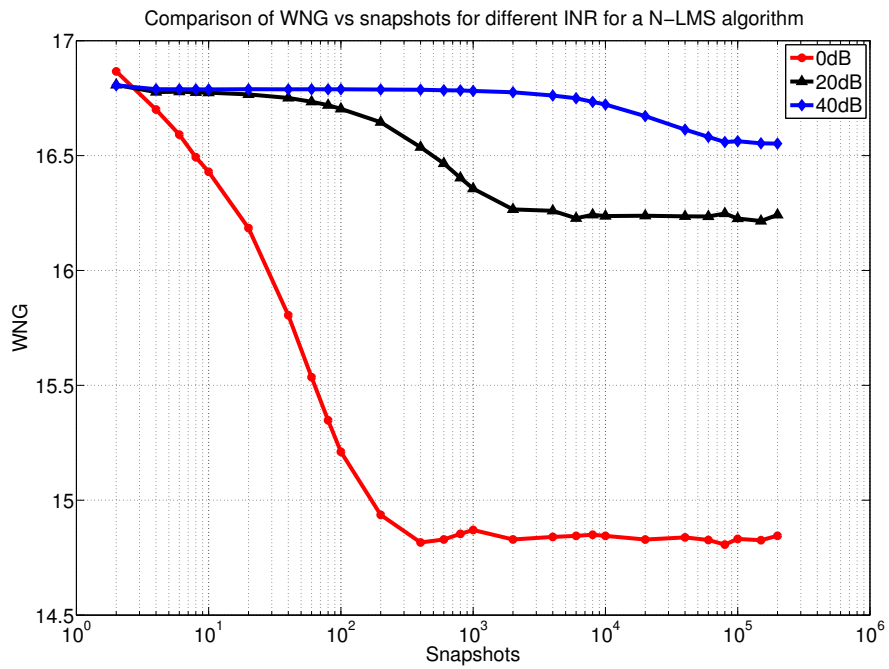


Figure 3.22: WNG comparison of N-LMS for the standard single interferer case with three INRs 0 dB, 20 dB and 40 dB. κ and sigma values are 1 and 1 respectively.

3.6 Summary

ND performance of Frost LMS algorithm depends on both interferer INR and step size μ . With a constant INR at the input the ND of Frost LMS algorithm decreases as step size μ decreases which is observed in Fig. 3.4. Firstly, for a constant INR and step size μ Frost LMS attains a constant ND value called as SSND. From the Fig. 3.4 40 dB INR interferer attains -92 dB and -60 dB for μ order of magnitude 9 and 6 respectively. Secondly, the speed at which Frost LMS attains SSND depends on the step size μ . Thus, lower step size μ means deeper SSND implies more number of snapshots. Further probing proves that Frost LMS takes an excess of 200,000 snapshots to attain the SSND of MVDR i.e. -127 dB for 40 dB. After analyzing the SSND vs μ curves for different INRs proves that SSND follows a linear trend presented in Eq. 3.4 as a function of μ . Comparing the cost of placing the notch, WNG, Frost LMS performance is similar to WNG of SD which is good. ND performance of N-LMS algorithm depends on INR of the interferer and step size parameter κ . Similar to Frost LMS SSND level of N-LMS decreases as the INR increases. However, for a constant INR SSND level decreases as the κ value decreases. For example Fig. 3.16 shows that 40 dB INR interferer SSND decreases from -50 dB and -70 dB for κ values of 1 and 0.01 respectively. Although N-LMS doesn't attain the SSND level of MVDR beamformer. Comparing ND performance of N-LMS and ER-DMR proves that ER-DMR algorithm attains deeper ND with less number of snapshots when compared to the N-LMS. For example Fig. 3.20 shows that ER-DMR attains a ND of -70 dB with just 100 snapshots while N-LMS takes 1000 snapshots to reach the same ND level. WNG performance of ER-DMR and N-LMS are the same however N-LMS attains a second WNG level for 40 dB INR interferer.

Chapter 4: Empirical Study of a Multi Interferer Case

Chapter 4 presents the comparison of empirical results of N-LMS and ER-DMR for the case of four interferers located in four peak side lobes of the CBF. Firstly an individual study of N-LMS and ER-DMR is performed and then the comparison of both the empirical results is presented in section 4.3.

4.1 Multiple Interferers Simulation Environment

The multiple interferer simulation uses an $N=50$ element array with half wavelength spacing. The interferers are located at four peak sidelobes: $u=0.06, 0.1, 0.14,$ and 0.18 . Fig. 4.1 illustrates the location of the interferers.

4.2 Results of N-LMS beamformer

The comparison of N-LMS performance, with a 40 dB INR at the first peak side lobe of a CBF is depicted in Fig. 4.2, with different INR levels in three other side lobe directions. In all the cases the value of κ is 1. The SSND level attained by the N-LMS algorithm is getting deeper with increase in the sum of the powers of four interferers in each of the four cases. Interestingly, the same behavior was observed in Fig. 3.20, in previous chapter, where the SSND level was getting lower as the κ value decreased from 1 to 0.01. Decreasing the κ value was decreasing the step size, which lead to the decrease in SSND level. Unlike the power at the input calculated for N-LMS for single INR in Eq. 4.3, the power of input here is comprised of four INR. As the sum of powers of interferers calculated in the adaptive step size μ is increasing the resultant step size μ at each step is decreasing. Thus, resulting in a decrease in SSND level and speed of convergence. Calculating the ensemble power at the

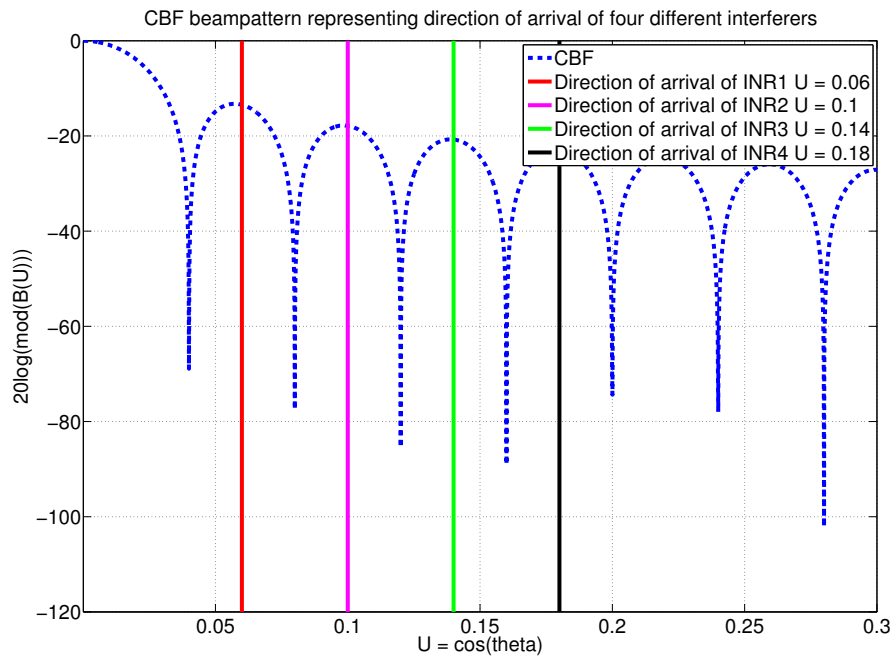


Figure 4.1: CBF beampattern with direction of arrival of different interferers. Four interferers arriving from direction corresponding to the u values of 0.06, 0.1, 0.14 and 0.18

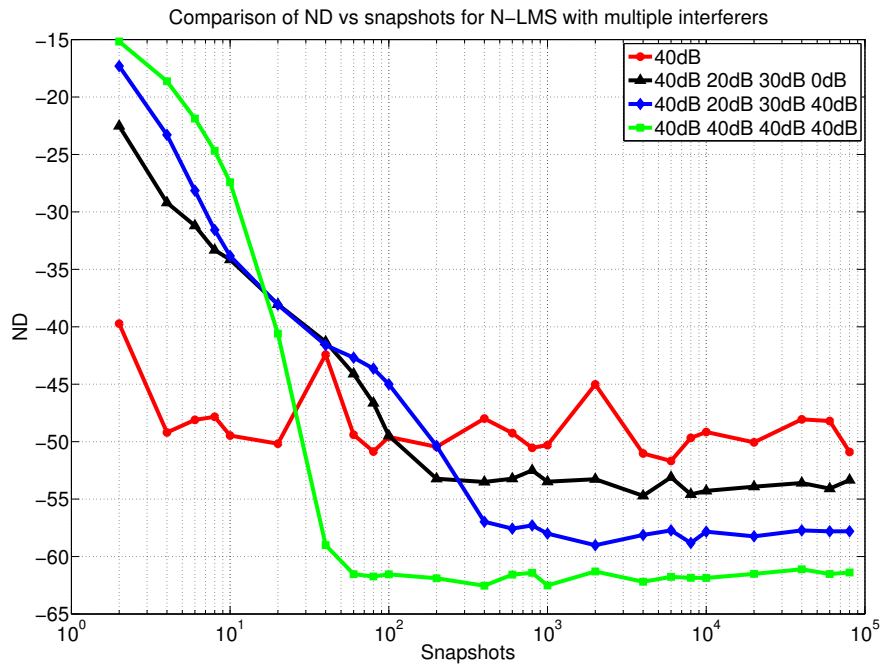


Figure 4.2: ND vs. snapshots performance comparison for robust LMS for the case of single and multiple interferers. Three different configurations of multiple interferers are used with four different INR power levels. All the interferers are incident from four consecutive peak side lobes of the CBF.

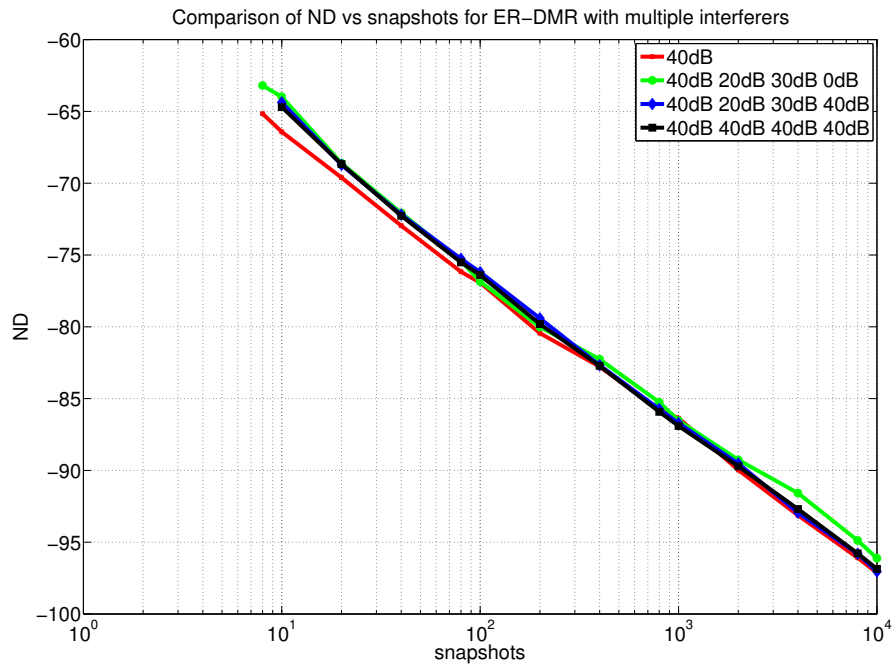


Figure 4.3: ND vs. snapshots performance comparison for ER-DMR for the case of single and multiple interferers. Three different configurations of multiple interferers are used with four different INR power levels All the interferers are incident from four consecutive peak side lobes of the CBF.

input makes this point more clear. As an example the ensemble value of the input power for the four interferer case with INR levels of 40 dB, 20 dB, 30 dB and 0 dB is calculated:

$$A = E[(b_{i1} * \mathbf{v}_{i1} + b_{i2} * \mathbf{v}_{i2} + b_{i3} * \mathbf{v}_{i3} + b_{i4} * \mathbf{v}_{i4})^H * (b_{i1} * \mathbf{v}_{i1} + b_{i2} * \mathbf{v}_{i2} + b_{i3} * \mathbf{v}_{i3} + b_{i4} * \mathbf{v}_{i4})]. \quad (4.1)$$

Since all the interferers are orthogonal to each other $\mathbf{v}_{im}^H * \mathbf{v}_{in} = 0$ for $m \neq n$ input power reduces to:

$$A = E[(b_{i1}^H * b_{i1} * \mathbf{v}_{i1}^H * \mathbf{v}_{i1}) + (b_{i2}^H * b_{i2} * \mathbf{v}_{i2}^H * \mathbf{v}_{i2}) + (b_{i3}^H * b_{i3} * \mathbf{v}_{i3}^H * \mathbf{v}_{i3}) + (b_{i4}^H * b_{i4} * \mathbf{v}_{i4}^H * \mathbf{v}_{i4})] \quad (4.2)$$

where b_{in} , for $n = 1,2,3,4$ are the zero mean complex circular random variables corresponding to four different interferers and $\mathbf{v}_{in}^H * \mathbf{v}_{in} = N = 50$ for $n = 1,2,3,4$. Applying expectation operator:

$$A = 50 * 10000 + 50 * 100 + 50 * 1000 + 50 * 1 = 555050. \quad (4.3)$$

Similarly, the value of A is 500000, 555050, 1055000, 2000000 for the four different cases in Fig. 4.2. As the value of A increases the value of μ decreases. As the interferer powers are increasing value of A is also increasing from 500000 to 2000000 thus decreasing the SSND level from -50 dB to -63 dB from case 1 to case 4. When the value of A increases by 1 order of magnitude in cases 3 and 4 compared to 1 and 2. This leads to a decrease in the SSND level further to -57 dB and -63 dB in cases 3 and 4, from -52 dB for cases 1 and 2 approximately. However the SSND level has some variance because the adaptive μ is changing at each snapshot. Thus, the increase in the number of interferers at the input is an important factor which contributes in the SSND level attained by the N-LMS algorithm. Understanding the behavior of NLMS for four interferers, the next step is to analyze the behavior of ER-DMR for multi interferer case.

4.3 Comparison of N-LMS and ER-DMR beamformers

Section 4.3 starts by analyzing the ND performance of ER-DMR for multiple interferer case. Further ND performance of N-LMS and ER-DMR are compared in Sections 4.3.1 and 4.3.2. In addition, computational complexity of N-LMS and ER-DMR are compared to observe the number of FLOPS (Floating point operations) required to compute the two algorithms at each snapshot. The number of FLOPS in turn helps in measuring the speed of convergence to ND for both the algorithms.

Fig. 4.3 depicts the performance of ER-DMR, with a 40 dB INR at the first peak side lobe of a CBF, with different INR levels in three other side lobe directions. Fig. 4.3 shows that ER-DMR could accurately estimate the eigenvectors and eigenvalues of the four interferers from SCM, in calculating the weight vector. Thus, ER-DMR performance remains independent of the interferer powers provided all the interferers arrive from the peak side lobes. The next section presents the comparison of DMR and LMS for multi interferer case.

4.3.1 Comparison based on Notch Depth

Fig. 4.4 presents the ND performance comparison of N-LMS and ER-DMR for the multi interferer cases. Two cases of INR levels are considered namely 40 dB, 20 dB, 30 dB, 0 dB and 40 dB, 40 dB, 40 dB, 40 dB at four different peak side lobes respectively. The SSND attained by N-LMS for both the cases is -55 dB and -60 dB. ER-DMR a ND of -65 dB with snapshots and decreases with increasing snapshots. In both the cases the performance of ER-DMR is far more better than that of N-LMS, similar to the single interferer case.

4.3.2 Comparison based on White Noise Gain

WNG comparison of N-LMS and ER-DMR algorithms is presented in Fig. 4.5. Clearly the cost of placing a notch for N-LMS is equal to that of ER-DMR. The Steady-state WNG attained for ER-DMR and N-LMS are 16.65 dB for the all the four different cases. Two

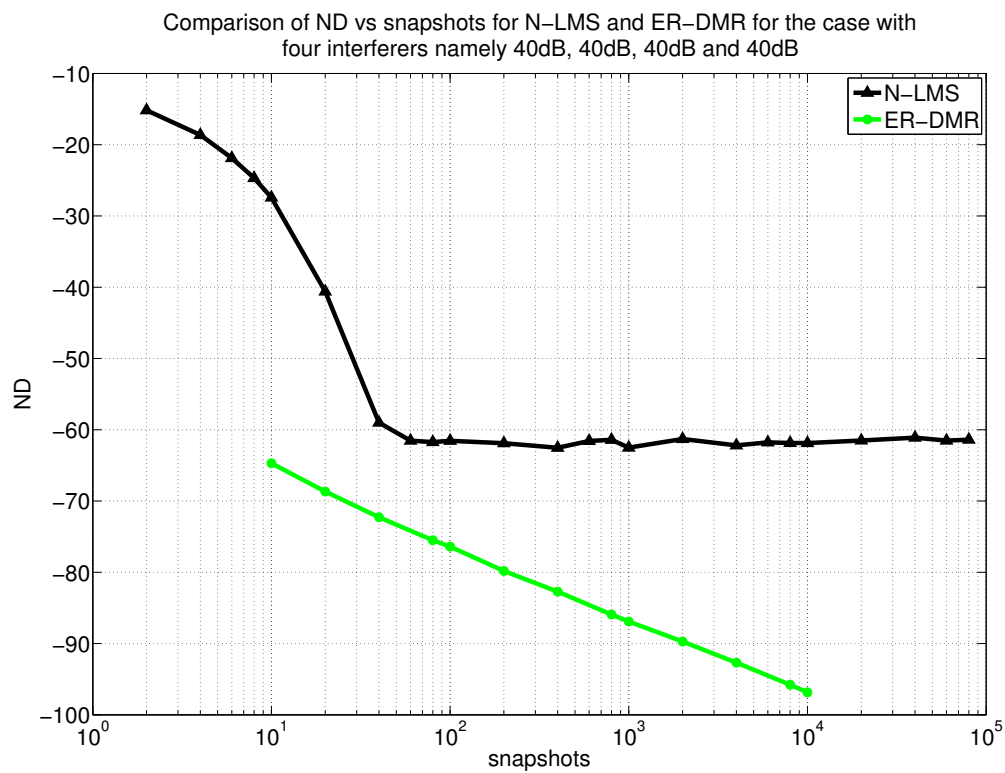
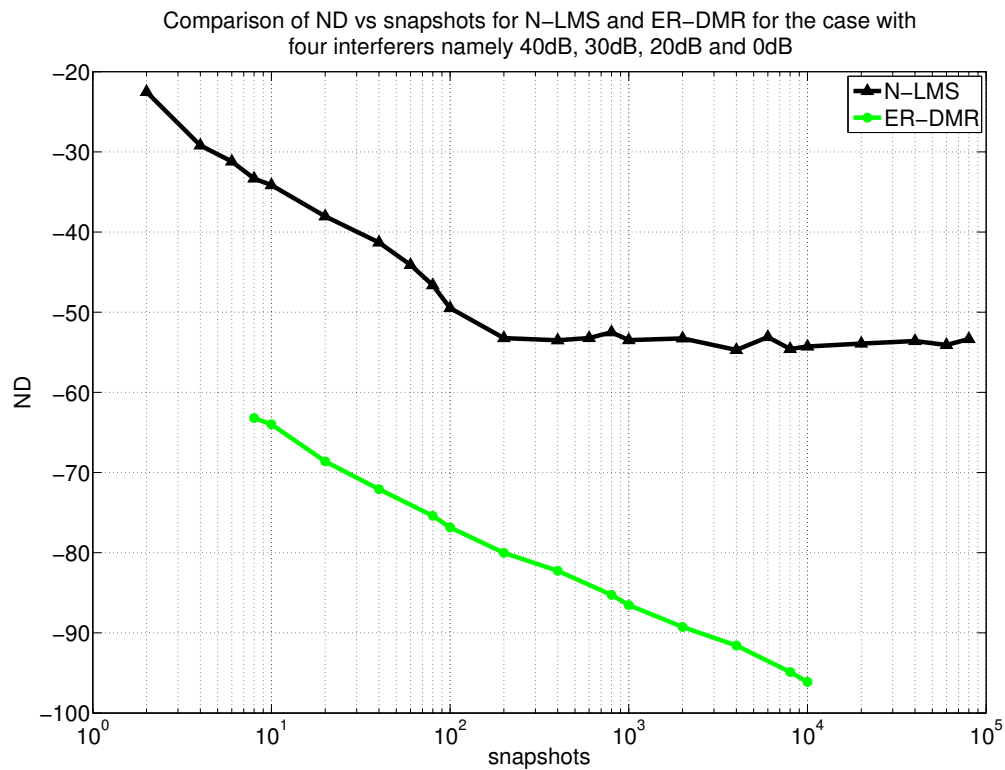


Figure 4.4: ND vs. snapshots performance comparison of ER-DMR and N-LMS for the case of multiple interferers. Four different INR power levels at four consecutive peak side lobes of the CBF. 40 dB, 20 dB, 30 dB and 50 dB INR's are used in the first comparison. 40 dB, 40 dB, 40 dB and 40 dB INRs are used in the second comparison.

conclusions could be drawn from the above analysis. First, the speed at which WNG is reaching a steady state value of 16.65 for both NLMS and ER-DMR is increasing with the total power at the input to the beamformer. Secondly, ER-DMR can achieve a deeper ND than N-LMS with the same constant WNG of 16.65 dB for all the three cases. Thus, in terms of WNG ER-DMR is efficient giving better performance than N-LMS. Sec. 4.4 compares the N-LMS and DMR beamformers in terms of computational complexity.

4.4 Computational Complexity of N-LMS and ER-DMR

Table 4.1 presents the FLOPS count, calculated theoretically, for N-LMS and ER-DMR for each function. The number of FLOPS are a function of number of sensors N . By plugging in four different values of N namely 20, 35, 50 and 75 we get the FLOPS count for NLMS and ER-DMR as shown in Table 4.2. The total count of FLOPS for N-LMS is on the order of N^2 , while DMR has FLOPS in the order of N^3 . In order to compare the N-LMS and ER-DMR performance a new term called the Multiplication Factor (MF) is introduced which is defined as the ratio of FLOPS count or execution time for ER-DMR and N-LMS. From the factors calculated for different N values it is clear that ER-DMR requires $N/3$ times more FLOPS than N-LMS which proves that N-LMS is faster than ER-DMR.

Table 4.1: Comparison of FLOPS count between N-LMS AND ER-DMR

FLOPS COUNT OF ER-DMR		FLOPS COUNT OF N-LMS	
Function	FLOPS	Function	FLOPS
Eigen decomposition	$2*(N^3)$	Calculating weight vector	$(6*N^2) + 10*N - 2$
Estimating dimension	$((9*N^2) + 23*N + 2)/2$		
Calculating weight vector	$(78*N) - 6$		
Total	$(4*(N^3) + (9*N^2) + 179*N - 10)/2$	Total	$(6*N^2) + 10*N - 2$

In order to verify the results through simulation, the `tic` and `toc` functions in Matlab are used to record the computation time t for 3000 snapshots. The time t is divided by 3000

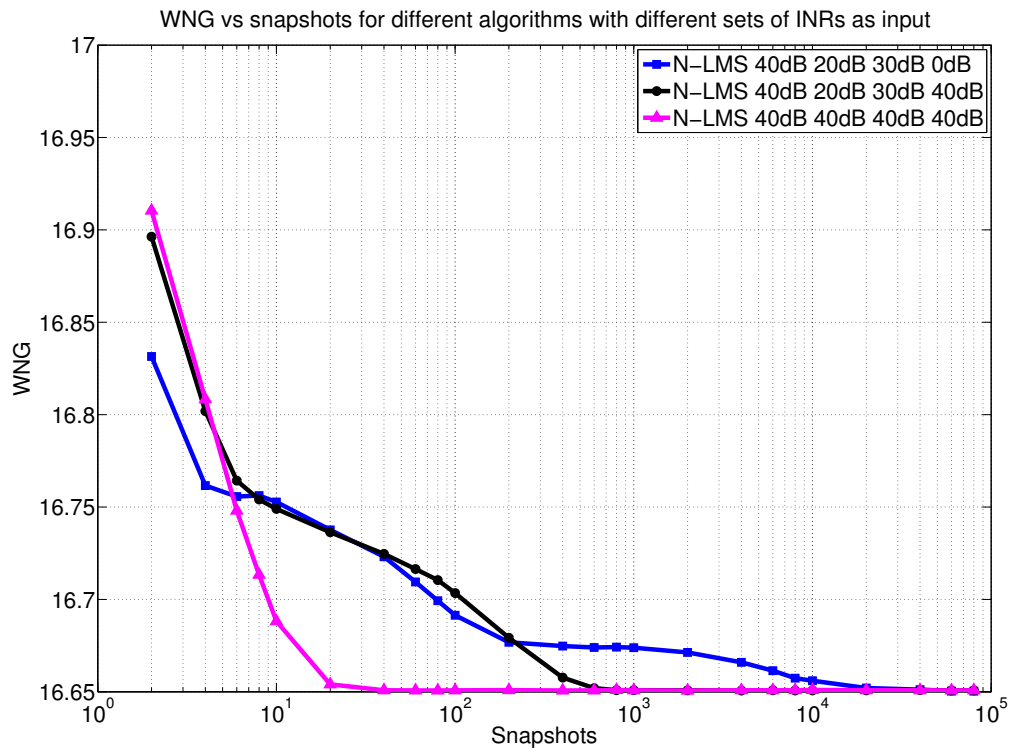
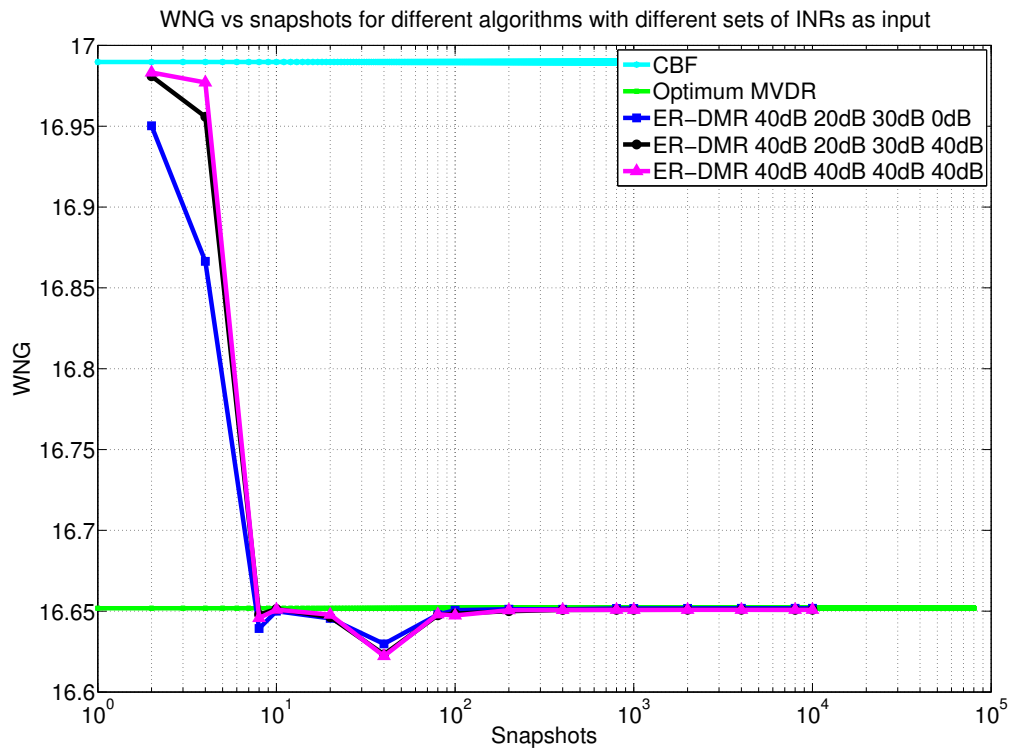


Figure 4.5: WNG vs. snapshots, cost comparison of ER-DMR and N-LMS for the case of multiple interferers. Four different INR power levels at four consecutive peak side lobes of the CBF.

Table 4.2: Theoretical Calculation of Multiplication factor for NLMS and ER-DMR

Multiplication factor for different array sizes			
N	FLOPS count for ER-DMR	FLOPS count for NLMS	MF
20	19585	2598	8
35	94390	7698	13
50	265720	15498	17
75	875770	34498	25

to obtain the average computation time for each time step. Similar to the MF calculation in Table 4.2, MF is calculated for each N . Simulation results in Table 4.3 show that the MF is not fixed but is varying based on the array size N . MF increases as N increases.

Table 4.3: Execution time comparison of NLMS and ER-DMR

Execution time at each step for different array sizes averaged over 3000 snapshots			
N	Execution time of ERDMR	Execution time of NLMS	MF
20	3.9438e-04	2.5064e-05	14
35	9.9064e-04	2.7122e-05	33
50	0.0018	2.7411e-05	56
75	0.0040	3.6646e-05	100

4.5 Summary

ND performance of ER-DMR is better than N-LMS for all the four multi interferer cases. Similar to the single interferer case ER-DMR attains a deeper notch with fewer snapshots when compared to the N-LMS beamformer. In addition, WNG of N-LMS and ER-DMR reach the same level of 16.65 dB for all the four multi interferer INR cases. ER-DMR takes $N/3$ times more FLOPS than the N-LMS beamformer for each snapshot.

Chapter 5: Conclusion

This thesis analyzed the performance of the constrained LMS beamformer proposed by Frost and compared it to the performance of the DMR beamformer proposed by Abraham and Owsley. Several performance metrics were considered, including notch depth, white noise gain, convergence speed, and computational complexity.

Chapter 3 of the thesis analyzed the performance of the LMS beamformer for a standard single interferer case, where the interferer is located at the peak sidelobe of the conventional beamformer. First the chapter analyzed the notch depth of the steepest descent beamformer, which relies on ensemble statistics to design the weight vector. For this beamformer, the notch depth is initially equal to that of the conventional beamformer. Given enough snapshots, the SD beamformer converges to the optimal notch depth. As expected, the gradient step size μ controls the convergence time of the steepest descent approach. Frost's LMS beamformer is the adaptive version of the SD beamformer that relies on an instantaneous estimate of the covariance, rather than ensemble statistics. Frost's standard algorithm uses a fixed step size. Chapter 3 showed that the notch depth of the Frost LMS beamformer follows the SD notch depth for low numbers of snapshots, but it eventually levels out at a steady state value that is significantly higher than the optimal value attained by steepest descent. This research showed that the SSND for the Frost algorithm is a linear function of the step size parameter. Results for the N-LMS algorithm, which uses an adaptive step size, are similar to the Frost algorithm. Comparing the N-LMS approach to the estimated rank DMR algorithm shows that DMR guarantees a significantly lower notch depth for all snapshots. The white noise gain of N-LMS and ER-DMR are comparable.

Chapter 4 presents an empirical study of the N-LMS and the ER-DMR beamformers for the case of multiple interferers. The results show that the DMR algorithm still guarantees significantly lower notch depths than the LMS algorithm. The higher performance of the DMR algorithm comes at the cost of higher computational complexity.

This thesis suggests several avenues for future work. First, it would be interesting to derive an analytical prediction of ND as a function of step size for the Frost LMS beamformer that could be compared to the empirical results presented in this thesis. Second, there are open questions about the white noise gain of the N-LMS beamformer for high numbers of snapshots. Finally, the analysis of computational complexity could be improved.

Bibliography

- [1] O. L. Frost, III, “An algorithm for linearly constrained adaptive array processing,” *Proc. IEEE*, vol. 60, no. 8, pp. 926–935, August 1972.
- [2] D. A. Abraham and N. L. Owsley, “Beamforming with dominant mode rejection,” in *Proc. IEEE Oceans*, 1990, pp. 470–475.
- [3] H. L. Van Trees, *Optimum Array Processing*. New York, NY: John Wiley and Sons, 2002.
- [4] K. E. Wage and J. R. Buck, “Snapshot performance of the Dominant Mode Rejection beamformer,” *IEEE Journal of Oceanic Engineering*, vol. 39, no. 2, pp. 212–225, April 2014.
- [5] J. R. Buck and K. E. Wage, “A random matrix theory model for the Dominant Mode Rejection beamformer notch depth,” in *Proc. IEEE Statistical Signal Processing Workshop*, August 2012, pp. 824–827.
- [6] K. E. Wage and J. R. Buck, “Convergence rate of the Dominant Mode Rejection beamformer for a single interferer,” in *Proc. International Conference on Acoustics, Speech, and Signal Processing*, May 2013, pp. 3796–3800.
- [7] B. Widrow and S. D. Stearns, *Adaptive Signal Processing*, 1st ed. Englewood Cliffs, NJ: Prentice-Hall, Inc., 1985.
- [8] R. A. Monzingo, R. L. Haupt, and T. W. Miller, *Introduction to Adaptive Arrays*, 2nd ed. Raleigh, NC: SciTech Publishing, Inc., 2011.

- [9] J. R. Treichler, J. C. Richard Johnson, and M. G. Larimore, *Theory And Design of Adaptive Filters*, 1st ed. Upper Saddle River, NJ: Prentice-Hall, Inc., 2001.
- [10] K. Wage and J. Buck, “Performance analysis of dominant mode rejection beamforming,” *International Congress on Acoustics*, 2010.
- [11] R. Nadakuditi and A. Edelman, “Sample eigenvalue based detection of high-dimensional signals in white noise using relatively few samples,” *Signal Processing, IEEE Transactions on*, vol. 56, pp. 2625 – 2638, July 2008.
- [12] G. C. Goodwin and K. S. Sin, *Adaptive Filtering Prediction and Control*, 1st ed. Englewood Cliffs, NJ: Prentice-Hall, Inc., 1984.
- [13] C. W. Therrien, *Discrete Random Signals And Statistical Signal Processing*, 1st ed. Englewood Cliffs, NJ: Prentice-Hall, Inc., 2001.

Biography

Mani S. K. Bojja grew up in Hyderabad, India. He attended the Jawaharlal Nehru Technological University (JNTU), where he received his Bachelor of Technology in Electronics and Communication in 2001. He went on to receive his Master of Sciences in Electrical Engineering from George Mason University in 2015.